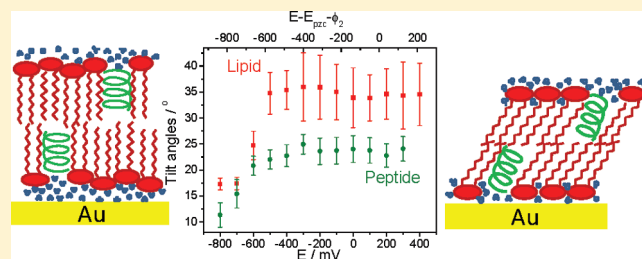


Electric Field Driven Changes of a Gramicidin Containing Lipid Bilayer Supported on a Au(111) Surface

Thamara Laredo,^{†,§} John R. Dutcher,[‡] and Jacek Lipkowski^{*,†}[†] Department of Chemistry and [‡] Department of Physics, University of Guelph, Guelph, Ontario, N1G 2W1, Canada

Supporting Information

ABSTRACT: Langmuir–Blodgett and Langmuir–Schaeffer methods were employed to deposit a mixed bilayer consisting of 90% of 1,2-dimyristoyl-*sn*-glycero-3-phosphocholine (DMPC) and 10% of gramicidin (GD), a short 15 residue ion channel forming peptide, onto a Au(111) electrode surface. This architecture allowed us to investigate the effect of the electrostatic potential applied to the electrode on the orientation and conformation of DMPC molecules in the bilayer containing the ion channel. The charge density data were determined from chronocoulometry experiments. The electric field and the potential across the membrane were determined through the use of charge density curves. The magnitudes of potentials across the gold-supported biomimetic membrane were comparable to the transmembrane potential acting on a natural membrane. The information regarding the orientation and conformation of DMPC and GD molecules in the bilayer was obtained from photon polarization modulation infrared reflection absorption spectroscopy (PMIRRAS) measurements. The results show that the bilayer is adsorbed, in direct contact with the metal surface, when the potential across the interface is more positive than -0.4 V and is lifted from the gold surface when the potential across the interface is more negative than -0.4 V. This change in the state of the bilayer has a significant impact on the orientation and conformation of the phospholipid and gramicidin molecules. The potential induced changes in the membrane containing peptide were compared to the changes in the structure of the pure DMPC bilayer determined in earlier studies.



INTRODUCTION

Ion channel forming peptides and proteins have various important biological functions, such as the transmission of information in the nervous system,¹ excitation of cells,² and antimicrobial activity.³ The antimicrobial activity of ion channel forming peptides has been recognized recently as a possible path for the treatment of antibiotic-resistant bacterial infections.^{4,5} Studies of the properties of peptides in a model membrane provide insight into the mechanisms of their antibiotic activity and can determine the type of cellular damage induced by peptides.⁵ These studies showed that there are definite relationships between membrane composition and peptide activity that could be relevant to the design and synthesis of new antimicrobial peptide pharmaceuticals.⁴ Additionally, studies of ion channels in lipid bilayers are of interest for the development of biochemical sensors.⁶ For these purposes, the structure and conformation of lipids and proteins in the membrane matrix have to be well understood.

The linear gramicidins are the best understood peptide antibiotics,^{7–10} and hence, they are ideal model systems to investigate the properties of this class of peptides in the lipid environment. Gramicidin is a 15 amino acid membrane spanning peptide that forms ion channels.^{11,12} In Gramicidin A, the amino acid sequence is as follows: HCO-LVal-Gly-LAla-DLeu-LAla-DVal-LVal-DVal-LTrp-DLeu-LTrp-DLeu-LTrp-DLeu-LTrp-NHCH₂CH₂OH. All of the residues in GD are neutral and

hydrophobic. Moreover, they alternate between *L*- and *D*-chiralities. These features of GD lead to the formation of helices that have a β -sheet hydrogen bonding pattern with all the residues projecting from one side of the sheet. These β -helices are characterized by a hydrophilic lumen formed by the backbone of the peptide while the residue side chains protrude outward and form the hydrophobic outer surface.¹³ The peptide structure displays polymorphism and, depending on the environment, forms either single-stranded or double-stranded helices denoted as β^m where m is the total number of residues (*L* plus *D*) per turn. Here, we will consider only the double-stranded $\beta^{5,6}$ and single-stranded $\beta^{6,3}$ structures. When $\beta^{6,3}$ gramicidin molecules are present in the two leaflets of a bilayer, they may form dimers that are stabilized by six hydrogen bonds between two N-end to N-end oriented molecules to create monovalent cation conductive channels spanning the membrane.^{7,8,14–16}

The conductivity of the gramicidin channels has been extensively investigated using bilayer lipid membranes (BLMs) formed in a small hole of a diaphragm separating two electrolyte solutions,^{7,8,14–16} in tethered^{17–19} or floating bilayers,^{20,21} supported on a gold electrode surface, or in phospholipid monolayers deposited on

Received: May 2, 2011

Revised: June 23, 2011

Published: June 27, 2011

the surface of a mercury electrode.^{22–27} These studies have established that in bilayers the channel is gated by formation of the dimer and that the conductance through the channel is dependent on the potential applied across the membrane. These studies involved only electrochemical measurements, and in the absence of additional molecular level information, their interpretation was based on modeling.

However, there is quite exhaustive literature describing NMR,^{28–30} X-ray scattering,³¹ and circular dichroism (CD)^{32,33} studies of gramicidin in phospholipid matrices in nonconductive samples such as stacks of multiple bilayers,^{28–30} bilayers supported on nonconductive surfaces,^{34–36} and solutions of vesicles.^{32,33} Several groups have studied membrane-bound GD samples using IR spectroscopy.^{35,37–46} There are two excellent reviews that describe these structural studies.^{7,47} It is now well established that the effect of gramicidin on the structure of phospholipid bilayers is similar to the effect observed upon addition of cholesterol.⁴⁸ The addition of GD increases (decreases) the percentage of gauche conformations in lipid chains at temperatures below (above) the phase transition temperature.^{42,49} Consequently, addition of gramicidin increases the tilt angle of the acyl chains and decreases the thickness of the bilayer in the gel state. In contrast, the tilt angle decreases and the thickness increases in the liquid crystalline state.^{7,47,50,51}

In addition, Ha et al.⁴³ performed PMIRRAS studies of GD incorporated into a hybrid hexadecanethiol/DMPC bilayer assembled at a gold electrode surface. These studies demonstrated that a bilayer containing GD can be investigated by PMIRRAS. However, these measurements were performed in air on dried samples and did not provide information about the effect of the electrode potential on the bilayer structure.

The present study describes *in situ* PMIRRAS experiments performed on a mixed DMPC/GD bilayer supported at a gold electrode surface and assembled into a spectroelectrochemical cell. The objective of this work is to obtain molecular-level information about the stability of the peptide-containing bilayer as a function of potential applied across the interface and about the orientation and the conformation of both the lipid and the peptide components of the membrane. In two recent papers,^{52,53} we have investigated the properties of gramicidin incorporated into a DMPC matrix supported at the Au(111) electrode surface. In the first paper, the matrix consisted of a monolayer of DMPC lipids and scanning tunneling microscopy (STM) was applied to image a single gramicidin molecule surrounded by the phospholipids.⁵² In the second paper, the matrix consisted of a stack of 10 bilayers supported at the gold electrode, and the potential induced changes in the peptide conformation and orientation were investigated with the help of circular dichroism (CD).⁵³ The objective of the present work is to complement the two previous studies by providing a description of the potential controlled changes in the structure of a single mixed DMPC/GD bilayer supported at the gold electrode surface. A single bilayer is too thick to be imaged by STM, and the amount of peptide in this bilayer is below the detection limit for the CD technique. Instead, the potential induced changes in the structure of the DMPC/GD bilayer were investigated using PMIRRAS. This technique has been successfully employed to characterize model biomimetic membranes supported at the gold electrode surface in several recent papers.^{54–67} We will provide new and unique information about the properties of the peptide containing membrane exposed to static electric fields that are comparable to the fields acting on a natural biological membrane.

This information will be useful in understanding the potential controlled conductivity of monovalent cations across the gramicidin channel.

EXPERIMENTAL SECTION

Reagents, Electrodes, and Thin Film Preparation Methods.

DMPC (1,2-dimyristoyl-*sn*-glycero-3-phosphocholine) and naturally occurring Gramicidin D (GD), which is a mixture of 80% gramicidin A, 5% gramicidin B, and 15% gramicidin C (Sigma-Aldrich, St. Louis, MO), were used without further purification to make 10 and 4 mg mL⁻¹ stock solutions, respectively, in dry trifluoroethanol (TFE) (Sigma-Aldrich). Volumes of both the lipid and peptide solutions were added to test tubes to an overall concentration of 10% molar ratio of GD with respect to DMPC. The tubes were then heated to about 40 °C for 1 h, during which time the solutions were vortex mixed (Fisher, Vortex Genie 2) at least once. The TFE was then evaporated from the test tubes by vortex mixing while a stream of argon flowed over the surface of the solution. This allowed for a thin film of the lipid-peptide mixture to remain as a coating on the inside walls of the test tubes. Further drying was achieved by storing the test tubes under vacuum for at least 12 h. These dry samples were then used either to prepare vesicle dispersions or as the initial material to spread DMPC/GD monolayers at the air/water interface. The Barenholtz procedure⁶⁸ was used to prepare vesicles for circular dichroism and transmission experiments: 1 mL of water or deuterated water (D₂O, Cambridge Isotope Laboratories, Cambridge MA, USA) was added to the test tubes and these were then sonicated (Aquasonic 50D, VWR Scientific Products, West Chester, PA) at the highest setting for 60 min at 50 °C. This procedure gave optically clear dispersions of vesicles. In order to make a monolayer at the air/water interface, the dry film in the test tube was redissolved in chloroform (Sigma-Aldrich) and a few drops of this solution were spread at the surface of a water-filled Langmuir-Blodgett trough (KSV LB5000, Finland) equipped with a movable barrier and a Wilhelmy plate to form a monolayer. The trough was controlled by a computer using the KSV LB5000 v 1.70 software. The temperature of the subphase was 19 ± 1 °C. Dissolution of GD molecules into the aqueous subphase was negligible at this temperature. The solvent was allowed to evaporate and the compression isotherm was recorded. The monolayers were transferred from the air/water interface onto the Au(111) electrode at surface pressures equal to 40 mN m⁻¹, corresponding to the mean molecular area of 53 Å². A combination of the Langmuir-Blodgett (LB) and the Langmuir-Schaeffer (LS) techniques was employed to fabricate the phospholipid bilayer on the Au(111) single crystal grown, cut, and polished in our laboratory. The first monolayer was transferred using the LB method by vertically withdrawing the electrode at the speed of 32 mm min⁻¹. The transfer ratio was 1.0 ± 0.1.

After immersion, the gold electrode covered by the monolayer was dried in air for at least 1 h. The second leaflet was transferred using the LS technique. The electrode covered by the first DMPC/GD layer was brought into horizontal contact with the monolayer of the DMPC/GD spread at the surface of the Langmuir trough and compressed to a preset surface pressure of 40 mN m⁻¹. The electrode covered by the bilayer was then detached from the aqueous subphase and dried in air overnight. Prior to any measurement, the bilayer-covered electrode was annealed in a dry atmosphere at 45 °C for 15 min. This provided a more uniform membrane as determined from AFM images shown in Figure SI 1 of the Supporting Information.

In all of our experiments, the working electrodes (WE) were Au(111) single crystals grown, cut, and polished in our laboratory.^{69,70} The counter electrode (CE) used for electrochemical measurements was a Au coil and the CE used for infrared measurements was a cylindrical Pt foil. Before each experiment, the Au electrodes were cleaned by flame-annealing and quenching with pure water, as described previously.⁷¹ The Pt electrode was sealed into the IR cell and cleaned together with the cell.

The reference electrode (RE) used for the electrochemical measurements was a saturated calomel electrode (SCE), placed in a separate vessel containing saturated KCl solution and connected to the cell with a salt bridge. The RE used in the infrared cell was a Ag/AgCl electrode (with a potential of -42 mV with respect to the SCE electrode) connected to the cell via a salt bridge with a Luggin capillary. All potentials in this paper will be quoted with respect to the Ag/AgCl reference electrode unless otherwise stated. Prior to experiments, all glassware was cleaned by immersion in a hot mixture of concentrated nitric and sulfuric acids (ratio 1:3) for at least 1 h. After cooling, it was rinsed with copious amounts of pure water, purified by a Milli-Q UV Plus (~ 18.2 M Ω cm) water system (Millipore, Bedford, MA). The electrochemical cell was then soaked in pure water for several hours and rinsed again. For all experiments, 0.1 M NaF (Merck, Suprapur) solutions were used as the supporting electrolyte. The presence of fluoride ions was needed to suppress dissolution of the BaF₂ window used in the PMIRRAS experiments.

Electrochemical Measurements. The electrochemical measurements were carried out in an all-glass three-electrode cell using the hanging meniscus configuration.⁷¹ The cleanliness of the NaF electrolyte was checked by cyclic voltammetry and differential capacitance (DC) measurements.

A computer-controlled system, consisting of a HEKA potentiostat/galvanostat, a HEKA (Lambrecht/Pfalz, Germany) scan generator, and a lock-in amplifier (EG&G Instruments 7265 DSP), was employed to perform electrochemical experiments. All data were acquired via a plug-in acquisition board (National Instruments PCI 6052E) using custom-written software generously provided by Professor Dan Bizzotto from the University of British Columbia.

In addition, chronocoulometry was employed to determine the charge density at the electrode surface. In this series of experiments, the Au(111) electrode was held at a base potential $E_{\text{base}} = -200$ mV for 120 s. Then, the potential was stepped to a variable value of interest starting from the most positive potential E_c and kept constant for another 120 s. To desorb the bilayer from the electrode surface, the potential was stepped to $E_{\text{des}} = -1250$ mV. The current transient corresponding to the desorption of the DMPC/GD bilayer was measured during 0.15 s. The time constant of the cell was about 0.003 s. Therefore, the interval 0.15 s was long enough to charge the interface and lift the bilayer and short enough for the charge corresponding to a hydrogen evolution to be small. The charge due to hydrogen evolution was subtracted using the procedure described in refs 69 and 71. The potential was then stepped back to the base value of $E_{\text{base}} = -200$ mV. Integration of the current transients gives the difference between charge densities at potentials E_c and E_{des} . This procedure was repeated three times for each point of the chronocoulometric curve with a freshly prepared bilayer. For the film free electrode in pure supporting electrolyte, all the points were collected in a single run. The absolute charge densities were then calculated using the independently determined potential of zero charge (pzc) $E_{\text{pzc}} = 215$ mV vs Ag/AgCl.

Spectra Collection and Processing. A Thermo Nicolet Nexus 8700 (Madison, WI) spectrometer, equipped with an external tabletop optical mount, High D*MCT-A detector, photoelastic modulator (PEM; Hinds Instruments PM-90 with II/ZSS0 ZnSe 50 kHz optical head, Hillsboro, OR), and demodulator (GWC Instruments Synchronous Sampling demodulator, Madison, WI) was used to perform the PMIRRAS experiments. The spectra were acquired using in-house software, an Omnic macro, and a digital-to-analog converter (Omega, Stamford, CT) to control the potentiostat (HEKA PG28S, Lambrecht/Pfalz, Germany) and to collect spectra. The IR window was a BaF₂ 1 in. equilateral prism (Janos Technology, Townshend, VT). Prior to the experiment, the window was washed in water and methanol and then cleaned for 30 min in an ozone chamber (UVO-cleaner, Jelight, Irvine, CA). The spectroelectrochemical cell was assembled and the Au(111) electrode covered by the bilayer formed by the LB-LS method was inserted into the cell. In these measurements,

the 0.1 M NaF supporting electrolyte solutions were made with deuterated water and all glassware was thoroughly dried before use. Solutions were purged of oxygen by bubbling with argon for at least 45 min, and an argon blanket was maintained throughout the experiment. A starting potential $E = 400$ mV vs Ag/AgCl was applied to the gold electrode, and 4000 spectra per applied potential step were collected. The potential was changed in steps of 100 mV in the negative direction to a value of -800 mV vs Ag/AgCl. The instrumental resolution was 2 cm^{-1} .

Measurements of IR spectra were carried out with the PEM set for half-wave retardation at 2900 cm^{-1} for the CH stretching region, and the angle of incidence of the infrared beam was set to 53.5°. The electrolyte thickness between the electrode and the prism was ca. 2.6 μm , giving the highest enhancement of the p-polarized light at the electrode surface. For the amide I and C=O stretching region, the maximum PEM efficiency was set to 1600 cm^{-1} . The angle of incidence was 60.5° and the electrolyte thickness was ca. 3.2 μm . In all cases, the thickness of the thin layer was determined by comparing the experimental reflectivity spectrum of the thin layer cell, attenuated due to the layer of solvent between the electrode and the IR window, to the reflectivity curve calculated from the optical constants of the DMPC/GD bilayer and of the cell constituents, as described in ref 72.

A modified version of a method described by Buffeteau et al.⁷³ was used to correct the average intensity $(I_s(\omega) + I_p(\omega))/2$ and the intensity difference $(I_s(\omega) - I_p(\omega))$ for the PEM response functions and for the difference in the optical throughputs for p- and s-polarized light ($\sim 6\%$).⁷⁴ The demodulation technique developed in Corn's laboratory^{75,76} was used in this work. Finally, the measured spectra had to be background-corrected due to the absorption of IR photons by the solvent in the thin-layer cavity. The spline interpolation technique described by Zamlynny et al.⁷⁴ was used for this background correction. When all of these corrections are introduced, the background-corrected spectrum is a plot of the wavenumber dependence of ΔS , which is proportional to the absorbance A of the adsorbed molecules

$$\Delta S = \frac{2(I_s - I_p)}{I_s + I_p} \approx 2.3\Gamma\epsilon = 2.3A \quad (1)$$

where Γ is the surface concentration of the adsorbed species and ϵ is the decimal molar absorption coefficient of the adsorbed species.

Spectral Deconvolution and Peak Assignment. The number of peaks under a spectral region and their corresponding position is determined through the combination of Fourier self-deconvolution (FSD) and two-dimensional correlation spectroscopy (2D-COS). We have used the FSD tool in OMNIC v 6.0a (Thermo software) with a typical bandwidth between 10 and 12 cm^{-1} and an enhancement usually set at 1.5 or less. Bandwidth here refers to an estimation of the width of the overlapped peaks, whereas enhancement refers to the degree to which the spectral features are resolved and it can be set between 1 and 5. The values of these two parameters were determined as the minimum value that, when combined, would not give negative side lobes in the FSD spectrum. This procedure was done for several spectra of the same set of experiments to diminish the uncertainty of the determination. For the 2D-COS, we have used the freeware 2DShige v 1.3 (Shigeaki Morita). In our case, the external perturbation consisted of a variable potential applied to the electrode. The reference spectrum for all experiments was that collected at -800 mV vs Ag/AgCl, which corresponds to the most negative potential of each set. From this analytical procedure, one obtains a synchronous and an asynchronous spectrum. We have used mainly the synchronous component for both peak determination and to establish correlations between the different peaks with the aim of obtaining sequential information. We have not interpreted the asynchronous component of the correlation due to complicated patterns that arise from the fact that our peaks shift as a function of potential. This issue has been addressed by several authors and in particular by Czarnecki.⁷⁷ Once the

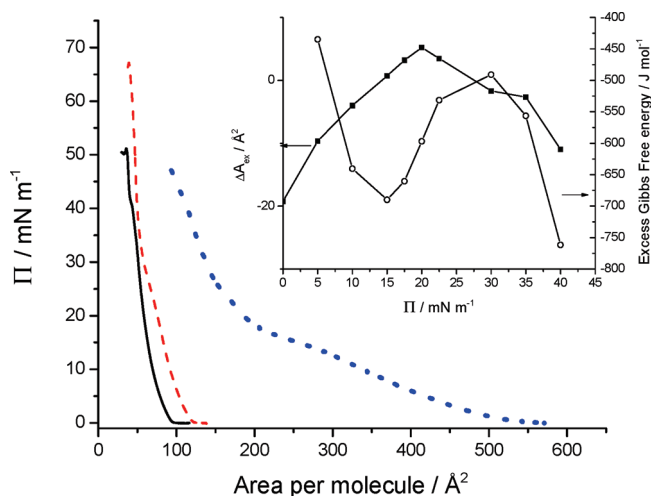


Figure 1. Compression isotherm at the air/water interface of DMPC (solid line) and DMPC/GD (dashed line) monolayers at 19 °C, and a GD monolayer (dotted line) at 20 °C (data for pure gramicidin taken from Weiss et al.³⁴). The inset shows the excess area (filled squares) and excess Gibbs free energy (empty circles) as a function of surface pressure calculated using eqs 2 and 3.

number of peaks and their positions agree for the two independent determinations, FSD and 2D-COS, we assign the peaks to their corresponding modes of vibration based on published literature on similar systems.^{78,79} Lastly, using *PeakFit* v 4.12 (Seasolve software), we fit all the peaks of the spectral region using mixed Lorentzian bandshapes to a deconvolution with an R^2 value of at least 0.99. The positions for all peaks were restricted to ± 3 cm^{-1} of the initial value determined from FSD and/or 2D-COS, which is usually the variation between the values determined using the two procedures.

RESULTS AND DISCUSSION

DMPC/GD Compression Isotherm. Figure 1 depicts the compression isotherm at the air/water interface of a DMPC/GD monolayer at 19 °C. For comparison, the isotherm of pure DMPC (our data) and the isotherm of pure GD taken from ref 34 (numerical data kindly provided by T. Hianik) are also shown in this graph. For the peptide-containing monolayer, compression starts at ~ 125 \AA^2 per molecule. Initially, the monolayer exists in the liquid-expanded phase in which the film pressure increases slowly with decreasing area per molecule. A phase transition from the liquid-expanded to the liquid-condensed phase occurs at ~ 80 \AA^2 and a film pressure of 20 mN m^{-1} . There is a further compression of the monolayer at a film pressure of 35 mN m^{-1} , corresponding to an area per molecule of 55 \AA^2 . The monolayer then collapses at a film pressure of ~ 65 mN m^{-1} . With respect to the pure DMPC and pure GD curves, it can be seen that the molecular area of the mixed monolayer is larger than that of the pure lipid and smaller than of the pure peptide for all film pressures. Information concerning the miscibility of the two components of the monolayer may be obtained from the change in the area at constant temperature and film pressure. The excess area of the mixture, ΔA_{ex} is defined as

$$\Delta A_{\text{ex}} = A_{12} - x_1 A_1 - x_2 A_2 \quad (2)$$

where A_{12} is the molecular area in the mixed monolayer at temperature T and surface pressure Π , A_1 and A_2 are the molecular areas in the pure component monolayers, and x_1 and x_2 are

the molar ratios of the two components of the mixture. ΔA_{ex} is equal to zero for an ideal mixture or when molecules are not miscible. A negative excess area suggests a miscibility of the two molecules, whereas positive excess areas correspond to a phase separation of the individual components in the mixed monolayer.³⁴ Using the compression isotherms in Figure 1, the excess areas for the mixed monolayer were calculated and were plotted as a function of the film pressure in the inset to Figure 1. In these calculations, we assumed that the solubility of the two components in the aqueous subphase is negligible and that the composition of the film is equal to the composition of the spreading solution (for membrane lipids, the solubility is in the range 10^{-10} to 10^{-12} M,⁸⁰ and for gramicidin, it is approximately 10^{-8} M⁴²). The excess areas are negative at film pressures less than 15 and higher than 25 mN m^{-1} , indicating that GD is miscible in the DMPC matrix at the air/water interface, even in the gel phase of the lipid at these film pressures. This result is in good agreement with the work of Weiss et al., where the excess area of several mixtures of different DMPC/GD ratios in the gel phase was determined to be negative at higher film pressures.³⁴

In addition, the excess Gibbs energy of mixing can be calculated by integration of the excess area versus film pressure plot using the formula³⁴

$$\Delta G_{\text{ex}} = \int_0^{\pi} \Delta A_{\text{ex}} d\pi \quad (3)$$

The calculated ΔG_{ex} values are also plotted in the inset to Figure 1. These values are negative in the whole range of film pressures investigated. However, they are smaller than the thermal energy $RT \approx 2.4$ kJ mol^{-1} indicating that the interactions between the components of the mixture are very weak. The most negative value of ΔG_{ex} is observed at a film pressure of 40 mN m^{-1} , indicating that a good miscibility of the two components is expected at this film pressure.

On the basis of the excess Gibbs energy of mixing analysis, the film pressure was selected to be 40 mN m^{-1} for the transfer of the monolayer from the air/water onto the gold electrode surface. At this value of the film pressure, the monolayer should be homogeneous. Indeed, our recent STM studies⁵² demonstrated that GD molecules are well-dispersed between DMPC molecules in the monolayer transferred at this film pressure. Previous studies with pure DMPC^{57,59} and DMPC mixed with cholesterol⁵⁴ were also performed with bilayers transferred onto the gold electrode at this value of the film pressure. All monolayers were transferred with the transfer ratio 1.0 ± 0.1 . The average area per molecule at this value of Π is ~ 53 \AA^2 .

Electrochemistry. Figure 2 plots the charge density versus potential curves determined from chronocoulometric experiments for the bare Au(111) electrode and the electrode covered by the DMPC/GD bilayer transferred at a surface pressure of 40 mN m^{-1} . The plot shows that the DMPC/GD bilayer is adsorbed onto the electrode surface in the region between -400 mV and 100 mV vs Ag/AgCl. At the most negative potentials between -1200 and -950 mV, the charge density curves corresponding to the surface covered by the bilayer and the film free electrode merge, indicating that the film is desorbed from the metal surface in this range. Independent neutron reflectivity (NR) experiments on similar systems demonstrated that in this state the film is detached from the electrode surface but remains in its close proximity, separated from the metal by a cushion of electrolyte ~ 1 nm thick.^{81,82} The NR experiments have also shown that the potential controlled

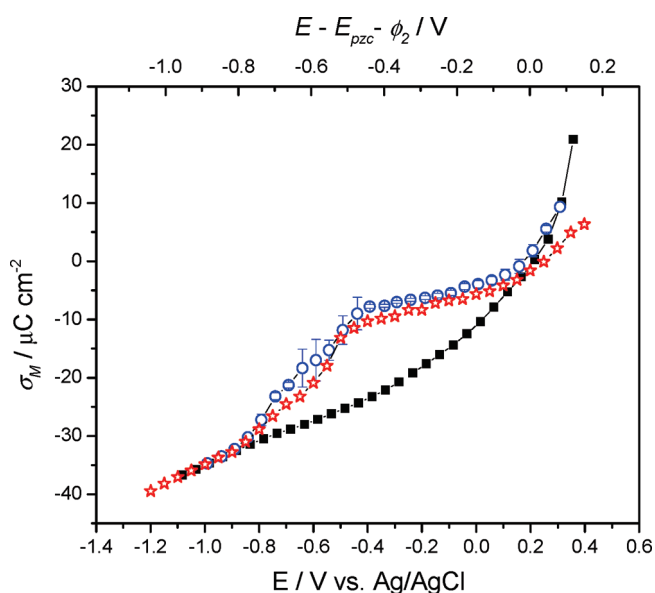


Figure 2. Charge density curves vs potential determined from chronocoulometric experiments for the film free Au(111) electrode (circles) and the electrode covered by the DMPC/GD bilayer (stars) transferred at a surface pressure of 40 mN m^{-1} .

detachment (dewetting of the film) is progressive. In the present case, the dewetting of the electrode surface from the bilayer could be seen as a step at $-800 \text{ mV} < E < -500 \text{ mV}$ on the charge density curve.

The GD channel is selective to cations. In 0.1 M NaF solution, it could be occupied by a single Na^+ ion.^{83,84} In that case, GD containing a sodium ion would be positively charged and the E_{pzc} should shift in the positive direction and the charge measured in the presence of GD should be more negative than for the pure DMPC bilayer. The star symbols in Figure 2 plot the charge density curve for the electrode covered by a pure DMPC bilayer assembled using the same procedure. The two charge density curves are very similar, and the charges measured in the presence of GD are even slightly more positive than in the absence of GD, although such a small difference may be a result of a small variation in the transfer ratio when the monolayers were transferred from the air solution interface onto the electrode surface using the LB-LS procedure. We reported that the transfer ratio was 1.0 ± 0.1 . Hence, we may exclude sodium incorporation into the channel.

Knowing the E_{pzc} of the bilayer covered electrode, one can also calculate the potential drop across the membrane as $(E - E_{\text{pzc}} - \phi_2)$, where ϕ_2 is the outer Helmholtz plane potential. The values of ϕ_2 were calculated from the charge density data using the diffuse layer theory.⁸⁵ The values of the potential drop across the interface are plotted in Figure 2 on the top horizontal axis. They represent the potential drop across the membrane due to the charge at the metal surface, when the bilayer is adsorbed on the metal. The data in Figure 2 indicate that the bilayer is adsorbed at the gold surface when the potential drop across the membrane is between ~ -0.4 and $\sim 0 \text{ V}$. Taking the thickness of the bilayer to be $\sim 5 \text{ nm}$, one can estimate that the bilayer is adsorbed on the metal when the static electric field is less than $1 \times 10^8 \text{ V/m}$. These fields are comparable to the fields acting on a natural biological membrane.⁸⁶

Spectroelectrochemistry. In this section, we describe the effect of the electric field with a magnitude comparable to the

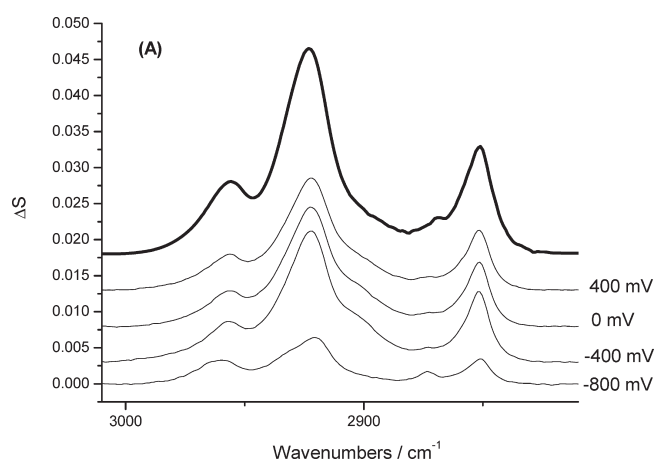


Figure 3. PMIRRA spectra of the CH stretching region for DMPC/GD bilayers transferred onto the Au(111) electrode at a surface pressure of 40 mN m^{-1} and 19°C for selected potentials. The thick line corresponds to the spectrum calculated for hypothetically randomly oriented molecules in a 5.4-nm -thick bilayer.

field acting on a natural biological membrane on the orientation and conformation of DMPC and GD molecules in the supported lipid bilayer.

DMPC Acyl Chains. Figure 3 shows the PMIRRAS spectra of the CH stretching region for the DMPC/GD bilayer transferred onto the Au(111) electrode at a film pressure of 40 mN m^{-1} and 19°C , at the potentials marked on the figure. The thick line plots the spectrum calculated for a 5.4-nm -thick bilayer of hypothetically randomly oriented molecules adsorbed at the gold electrode surface. This spectrum was calculated by solving the Fresnel equations for the four-phase system: Au/DMPC/GD/ D_2O /BaF₂. The optical constants for the DMPC/GD film were determined from a transmittance measurement of a dispersion of DMPC/GD vesicles in D_2O using the procedure described in refs 74,87. They are reported in the Supporting Information, Figure SI 2.

The CH stretch region of the IR spectra consists of several overlapping bands. In order to perform quantitative analysis of these data, the spectra need to be deconvoluted. The Fourier self-deconvolution (FSD) and generalized two-dimensional correlation spectroscopy (2D-COS)⁸⁸ were used to identify bands present in this spectral region. The top panel in Figure 4 shows the deconvoluted spectrum based on the 2D synchronous correlation analysis (bottom panel). Four autocorrelation peaks observed at $\sim 2958, 2943, 2923,$ and 2852 cm^{-1} correspond to the methyl asymmetric stretch, $\nu_{\text{as}}(\text{CH}_3)$, the Fermi resonance between the symmetric methyl stretching and the methylene bending modes, and the methylene asymmetric $\nu_{\text{as}}(\text{CH}_2)$ and symmetric $\nu_{\text{s}}(\text{CH}_2)$ stretches, respectively.⁸⁹ The bottom panel in Figure 4 displays positive correlations at $(2958, 2923)$; $(2958, 2852)$; $(2923, 2873)$ $(2923, 2852)$, which imply that the two autocorrelated peaks change in the same direction as a function of applied potential. The autocorrelation peak corresponding to the Fermi resonance between the symmetric stretch and the bending mode of the methylene groups at $\sim 2902 \text{ cm}^{-1}$ cannot be easily identified from the synchronous spectra. However, such a peak can be resolved using the Fourier self-deconvolution procedure shown in Figure SI 3 of the Supporting Information. This example shows that 2D-COS alone does not provide complete band identification. The spectra were then deconvoluted using the same set of initial parameters. The deconvolution is highly

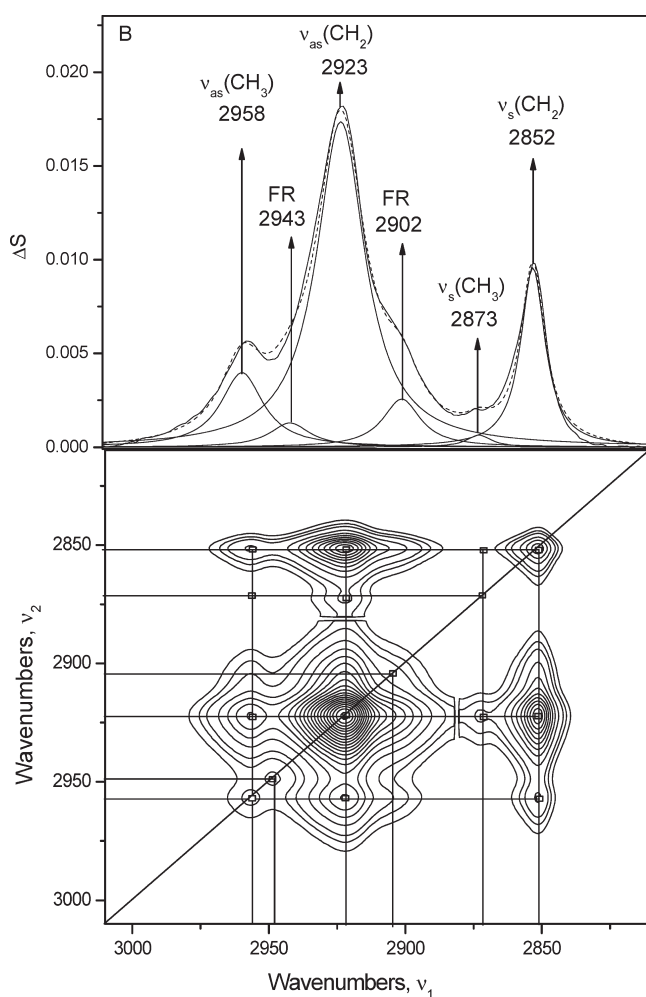


Figure 4. Deconvoluted spectrum of the CH stretching region for the DMPC/GD bilayer at $E = -0.4$ V (top panel) based on the 2D synchronous correlation spectrum (bottom panel). Four autopeaks can be observed at 2958, 2943, 2923, and 2852 cm^{-1} . There are positive correlations at (2958, 2923); (2958, 2852); (2923, 2873); and (2923, 2852).

dependent on the choice of the band shape of the individual peaks. We have used the Lorentzian function which was shown to give a good fit to the spectra of phospholipid bilayers supported at a gold electrode surface.^{54,57}

Structure of the Lipid Matrix. Figure 5A shows the frequency of the symmetric and asymmetric methylene stretching bands in the supported DMPC/GD bilayer as a function of the electrode potential. The peak positions correspond to the deconvoluted bands using the Lorentzian function. On average, the peak position for the DMPC/GD system is 2921.5 ± 0.5 cm^{-1} for $\nu_{\text{as}}(\text{CH}_2)$ and 2852 ± 0.5 cm^{-1} for $\nu_{\text{s}}(\text{CH}_2)$, a result that agrees with that found for pure DMPC⁵⁷ and DMPC/cholesterol⁵⁴ systems.

Frequencies of the band maximum lower than 2920 cm^{-1} for $\nu_{\text{as}}(\text{CH}_2)$ and 2850 cm^{-1} for $\nu_{\text{s}}(\text{CH}_2)$ are characteristic of the gel state of the bilayer in which the acyl chains are fully stretched and assume an all-*trans* conformation.^{90–92} The frequencies reported in Figure 5 are slightly higher than the values expected for the gel state indicating that the acyl chains have a certain percentage of *gauche* conformation. However, the band positions in the supported bilayer are red-shifted with respect to the frequencies of

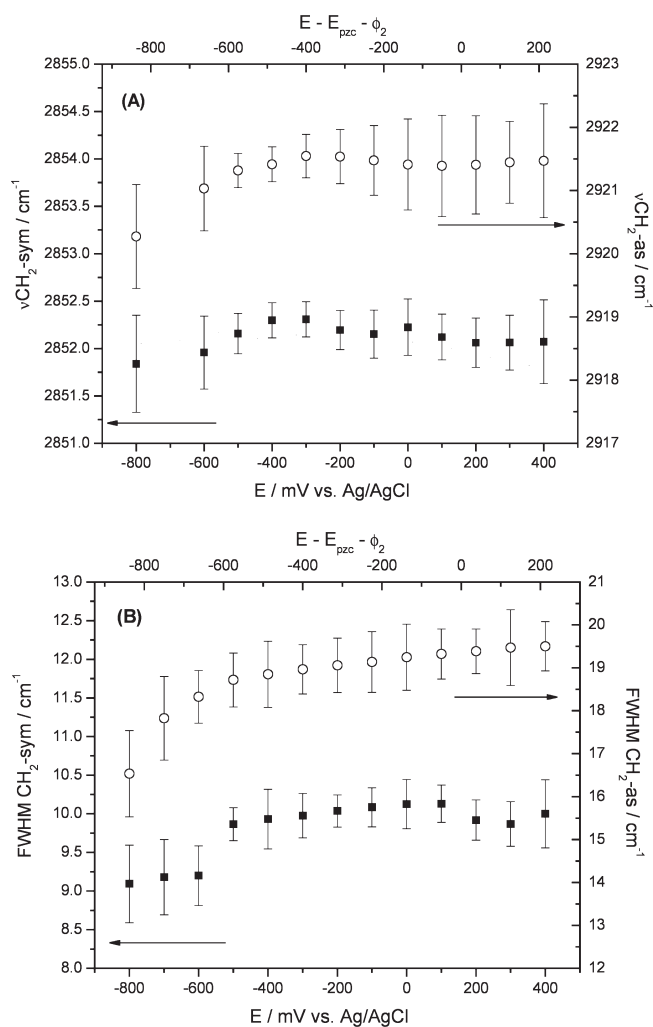


Figure 5. Change in frequency position (A) and fwhm (B) of the asymmetric (empty symbols) and symmetric (filled symbols) methylene stretching bands of the acyl chains of the lipid for the DMPC/GD bilayer. The error bars correspond to the standard deviation calculated from 3 independent measurements.

the corresponding bands in the suspension of vesicles which are 2924 ± 0.5 cm^{-1} for the $\nu_{\text{as}}(\text{CH}_2)$ and 2853 ± 0.5 cm^{-1} for the $\nu_{\text{s}}(\text{CH}_2)$. Hence, although not in a fully *trans* state, the *trans* to *gauche* ratio of the lipid chains is higher when the bilayer is supported on gold than in the vesicle. This property suggests that the supported bilayer is somewhat more ordered than the free-standing bilayer in vesicles. This is consistent with the PM-IRRAS studies by Garcia-Araez et al.⁵⁹ which have shown that the solid support has an influence on the ordering of DMPC molecules in the supported bilayer. The data in Figure 5A show also a weak dependence on the electrode potential. The peak positions shift to lower wavenumbers when the bilayer is detached from the gold surface at negative potentials. Although it is a small shift, it is larger than the error bars. It suggests a somewhat lower content of *gauche* conformers and hence a slightly more ordered state. The band frequencies are also slightly red-shifted at potentials close to the pzc indicating a small dependence of the order of the bilayer on the applied potential in the adsorbed state.

Figure 5B plots the potential dependence of the FWHM for the asymmetric and symmetric CH_2 stretches. These numbers are

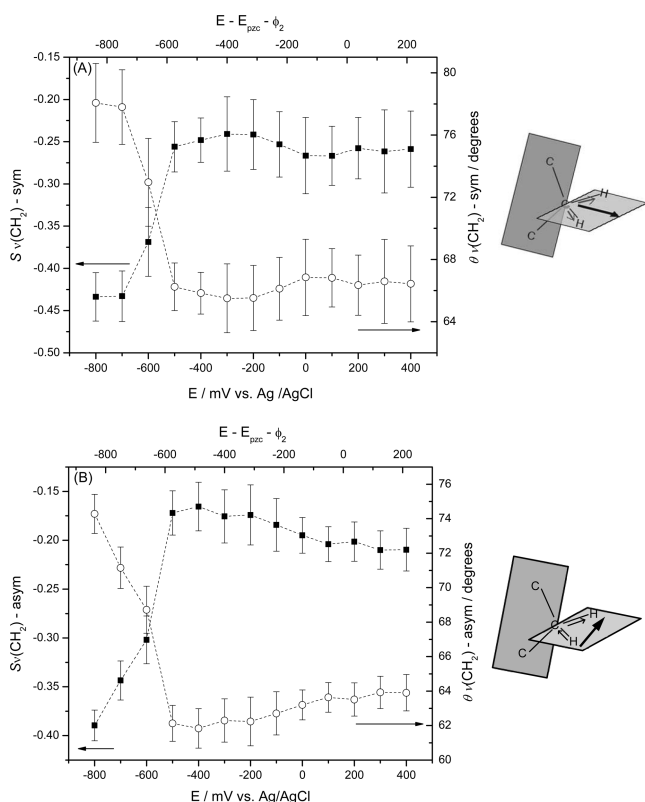


Figure 6. Dependence of the order parameter, S (filled squares), and tilt angle, θ (empty circles), with potential for (A) $\nu_{\text{sym}}(\text{CH}_2)$ and (B) $\nu_{\text{asym}}(\text{CH}_2)$. Cartoons show the direction of the transition dipole for the corresponding vibration. The error bars correspond to standard deviation calculated from 3 independent measurements.

1 to 2 cm^{-1} larger than for the bilayer of pure DMPC supported at the gold surface,⁵⁷ suggesting that the mobility of acyl chains is somewhat higher in the presence of GD. The bands are somewhat narrower in the desorbed state at $E = -0.8$ V versus Ag/AgCl suggesting that the chains are less mobile when the bilayer is separated from the metal by a thin layer of electrolyte.

Orientation of the Acyl Chains. At constant surface coverage, the integrated intensities of the IR absorption band are proportional to the square of the dot product of the vector of the transition dipole moment and the vector of the electric field of the photon $|\boldsymbol{\mu} \cdot \mathbf{E}|^2$, according to the formula^{93,94}

$$\int Adv \propto |\boldsymbol{\mu} \cdot \mathbf{E}|^2 = \langle \cos^2 \theta \rangle |\boldsymbol{\mu}|^2 \langle \mathbf{E} \rangle^2 \quad (4)$$

where θ is the angle between the two vectors, $|\boldsymbol{\mu}|^2$ is the square of the absolute value of the transition dipole, and $\langle \mathbf{E} \rangle^2$ is the mean square of the electric field of the photon. The spectra in Figure 3 show that intensities of the methylene stretching bands are dependent on the electrode potential. The electric field of the photon is perpendicular to the surface. Therefore, the integrated intensities of these bands may be used to calculate the angle θ between the direction of the transition dipole and the surface normal using the following equation:^{93,94}

$$\langle \cos^2 \theta \rangle = \frac{1}{3} \frac{A_{(\text{E})}}{A_{(\text{random})}} \quad (5)$$

where $A_{(\text{E})}$ and $A_{(\text{random})}$ are the integrated intensities of the bands in the bilayer at the gold surface and in a hypothetical bilayer of randomly distributed molecules. To determine θ , the spectrum for a film with randomly oriented molecules must be known. This spectrum was calculated from optical constants for DMPC/GD samples, assuming a total thickness of the bilayer of 5.4 nm. This procedure has been thoroughly explained elsewhere.⁷⁴

Figure 6A plots changes of the angle θ with potential for $\nu_{\text{s}}(\text{CH}_2)$ and Figure 6B plots the corresponding changes in θ for $\nu_{\text{as}}(\text{CH}_2)$. The angle between the directions of the transition dipole moments of both CH_2 vibrations changes from a value of $\sim 64^\circ$, at potentials where the bilayer is adsorbed and in direct contact with the metal surface, to $\sim 78^\circ$ at negative potentials where the bilayer is detached from the metal surface. The cartoons in Figure 6A show that the vector of the transition dipole of the symmetric stretch lies along the bisector of the CH_2 plane. The direction of the transition dipole of the asymmetric methylene stretch is along the line joining the two hydrogen atoms of the methylene group.^{78,79} It should be emphasized that these two angles do not need to be equal, because the acyl chains can assume an orientation in which the plane of the CH_2 group is tilted with respect to surface normal but also rotated with respect to the surface along the diagonal of the CH_2 moiety. Such rotation changes the angle of the asymmetric stretch and does not affect the angle of the symmetric stretch.

The CH_2 bending mode shows up as a single band at ~ 1468 cm^{-1} . The orientation of the transition dipole moment of this vibration has the same direction as that of the symmetric methylene stretch. Figure SI 4 of the Supporting Information shows that, indeed, similar values of the angle θ are determined from integrated intensities of the $\delta(\text{CH}_2)$ and the $\nu_{\text{s}}(\text{CH}_2)$ modes. Since the two spectral regions were studied independently, this agreement indicates that no major errors were made when performing the background correction and the deconvolution procedure.

The orientation of acyl chains is usually described in terms of the order parameter. For the direction of the dipole moment of an IR band, the order parameter is defined as⁹⁵

$$S_{\text{CH}_2} = \frac{1}{2} (3 \langle \cos^2 \theta \rangle - 1) \quad (6)$$

where $\langle \cos^2 \theta \rangle$ is determined from eq 5, and the angular brackets denote ensemble averaging over all absorbing dipoles in the sample. Equation 6 implies that the order parameter can have values that range between unity and -0.5 when the transition dipoles are oriented parallel or perpendicular with respect to the normal to the surface, respectively. When $S = 0$, the system is totally disordered and in random orientation with an average tilt equal to the magic angle (54.7°). The order parameter calculated with the help of eq 6 is plotted as a function of the electrode potential in Figure 6A,B for the transition dipoles of the symmetric and asymmetric CH_2 stretches, respectively. The values of the order parameter for $\nu_{\text{as}}(\text{CH}_2)$ and $\nu_{\text{s}}(\text{CH}_2)$ are -0.19 ± 0.02 and -0.26 ± 0.03 , respectively, for the adsorbed state of the DMPC/GD bilayer. Upon desorption, however, the magnitude of the order parameter changes to -0.39 ± 0.02 and -0.43 ± 0.03 for the $\nu_{\text{as}}(\text{CH}_2)$ and $\nu_{\text{s}}(\text{CH}_2)$ vibrations, respectively.

Since the angle between transition dipoles of CH_2 stretches and a *trans* fragment of the acyl chain is 90° , the order parameter of the transition dipoles can be used to calculate the order

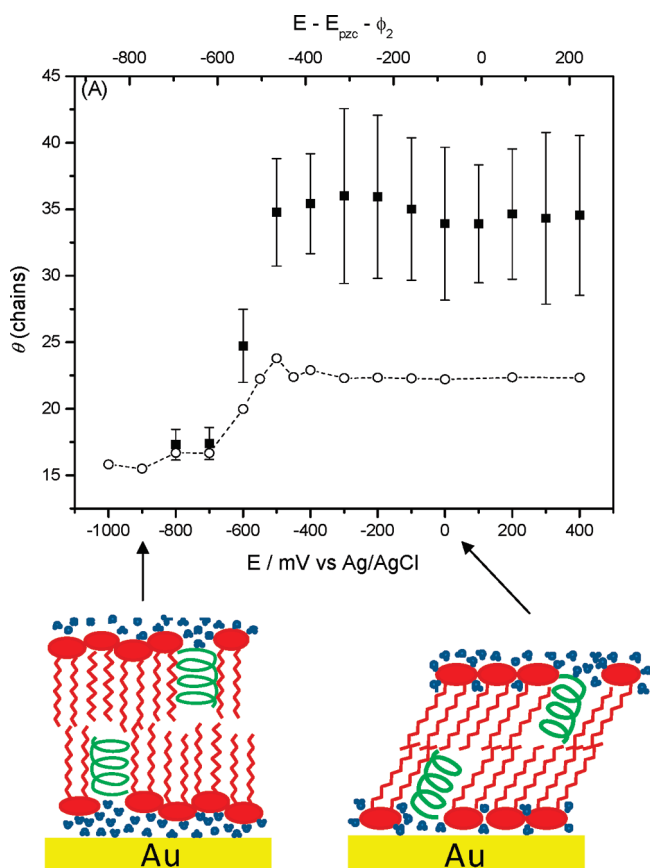


Figure 7. Orientation of the acyl chains in the DMPC/GD bilayer (filled squares) versus potential as calculated from the order parameter S_{CH_2} with the aid of eq 7. The error bars shown correspond to the standard deviation of 3 independent sets of data. The empty circles correspond to previous work on pure DMPC bilayers formed by the LB/LS technique.⁵⁷ The cartoons show how the lipids are arranged in a zigzag fashion when desorbed and in a planar geometry when adsorbed. Sketches of the two possible headgroup packing and chain tilts are based on models derived from the X-ray crystallographic studies of phospholipid bilayers (Hauser, H.; Pascher, I.; Pearson, R.H.; Sundell, S., Preferred conformation and molecular packing of phosphatidyl ethanolamine and phosphatidylcholine. *Biochim. Biophys. Acta*, 1981, 650, 21–51). The error bars were calculated using the procedure described in the Supporting Information.

parameter of the *trans* segments of the acyl chains using the transformation⁹⁶

$$S_{\text{chain}} = S_{\text{CH}_2} [(3 \cos^2 90 - 1)/2]^{-1} = -2S_{\text{CH}_2} \quad (7)$$

The order parameter, S_{chain} , is defined as

$$S_{\text{chain}} = \frac{1}{2}(3\langle \cos^2 \theta_{\text{chain}} \rangle - 1) \quad (8)$$

It is an average measure of the orientation of the chain segments that depends both on the chain tilt and on the amount of the *gauche* conformers in the acyl chains. The values of the acyl chain tilt in the DMPC/GD bilayer calculated from the intensity of the symmetric CH_2 stretch with the aid of eqs 6–8 are plotted versus the potential in Figure 7. The error bars correspond to the standard deviation obtained from at least 3 independent sets of data. The estimated error in the determination of $\langle \theta_{\text{chain}} \rangle$

due to the uncertainty of the background correction and band deconvolution procedures is $\pm 3^\circ$ as described in the Supporting Information.

The average tilt of the acyl chains in the DMPC/GD bilayer changes from about 35° in the adsorbed state to $\sim 18^\circ$ when it is detached from the surface. For comparison, the $\langle \theta_{\text{chain}} \rangle$ values calculated from the data by Zawisza et al.⁵⁷ for a pure DMPC bilayer are also included in Figure 7. The tilt angles display similar dependence on the electrode potential for the two bilayers. However, the tilt of the acyl chains is increased by about 10° in the adsorbed state and by about 2° in the desorbed state if GD is present in the bilayer. An increase of the chain tilt angle between 5° and 10° upon incorporation of GD into the stack of multiple bilayers was also observed in ATR studies by Bouchard and Auger.⁴⁶ This behavior is in accord with the ^2H NMR studies by Morrow and Davis⁹⁷ who have demonstrated that the S_{CD} parameter decreases upon addition of GD to a stack of multiple DMPC bilayers at temperatures below the phase transition. It is also in agreement with the X-ray diffraction studies by Harroun et al., who observed that the DMPC/GD (10:1 mol ratio) bilayer is thinner than the pure DMPC bilayer.⁹⁸ The thinning and hence the increase of the membrane tilt angle caused by the presence of GD may be explained by hydrophobic matching.⁴⁹ In the gel state, the thickness of the hydrophobic portion of the membrane is approximately 3.2 nm. The length of the GD helical dimer is approximately 2.6 nm.⁴⁷ The membrane becomes thinner and the tilt angle of the acyl chains increases in order to match the thickness of the membrane to the length of the channel.

A significant result of the present study is the information about the effect of the potential drop across the interface on the membrane structure and stability at the metal surface. The detachment of the membrane is seen in Figure 7 as a decrease of the tilt angle. As shown by neutron reflectivity experiments done on a similar system, a cushion of electrolyte of ~ 1 nm thickness exists between the bilayer and the electrode surface in the desorbed state.⁸¹ This allows for the lipid headgroup to pack in a tighter fashion, decreasing the average tilt of the acyl chains.^{54,57} Zawisza et al.⁵⁷ have shown that a tilt angle of $\sim 17^\circ$ corresponds to an area per molecule of $\sim 0.41 \text{ nm}^2$, which is expected for a DMPC bilayer in the gel state in which the polar heads are packed in a zigzag fashion, as illustrated schematically by the cartoon in Figure 7. The data in Figure 7 indicate that the structure of the bilayer is different for the adsorbed and desorbed states. In the adsorbed state, all polar heads are in contact with the metal and are located in one plane, occupying a larger surface area, as shown in the cartoon in Figure 7. To compensate for the increase in the head area, the chains tilt.⁵⁷ The large change of the tilt angle between the adsorbed and the desorbed states is driven by the difference in the packing of the polar heads of DMPC molecules in the two states. The data in Figure 7 show that the stability of the bilayer is comparable in the presence and in the absence of the peptide.

Figure 7 also shows that there are small but measurable changes of the tilt angle with potential for the bilayer in the adsorbed state. It was discussed above that $(E - E_{\text{pzc}} - \phi_2)$ may be used as an equivalent of the transmembrane potential applied to a membrane when the channel is not conductive. When a potential difference $(E - E_{\text{pzc}} - \phi_2)$ is applied to the membrane, it compresses the bilayer with a pressure p equal to⁹⁹

$$p = C(E - E_{\text{pzc}} - \phi_2)^2 / 2d \quad (9)$$

Table 1. Chain Order Parameter and Average Tilt Angle Values of *Trans* Chain Fragments Chain for DMPC in the Presence of GD Determined in Present Work, as well as Literature Values Obtained for Multiple Bilayers or Mixed Monolayers

sample	from $\nu(\text{CH}_2)$ -asym		from $\nu(\text{CH}_2)$ -sym		ref
	S_{chain}	$\langle\theta_{\text{chain}}\rangle$	S_{chain}	$\langle\theta_{\text{chain}}\rangle$	
DMPC/GD (30:1 mol ratio) – air-dried film of liposomes applied to CaF ₂ window measured by polarized IR in transmission at room temperature ^d	0.94	11.5°	0.94	11.5°	37
DMPC/GD (8:1 mol ratio)-monolayer at Ge crystal in solution, $t = 21$ °C, measured by ATR			0.60	31°	44
DMPC/GD (10:1 mol ratio) rehydrated multiple bilayers $t = 10$ °C, measured by ATR	0.52	34°	0.56	33°	39
DMPC/GD (between 10 and 8:1 mol ratio) dry multiple bilayers, room temperature, measured by ATR ^a	0.72	26°	0.72	26°	100
DMPC/GD (10:1 mol ratio) hydrated bilayers cast on a germanium ATR crystal, room temperature, measurements in air ^c			(0.51–0.63)	(29–34°)	46
			depending on the solvent from which bilayers were cast		
DMPC- <i>d</i> ₅₄ /GD (40:1 mol ratio), from C–D bond angles, dry multiple bilayers, $t = 19$ °C, NMR ^b			0.56	33°	97
present data at $E > -0.4$ V – adsorbed state	~0.4	39°	~0.5	35°	
present data at $E = -0.8$ V desorbed state	0.8	21°	0.85	18°	

^a Calculated from S_{CH_2} for $\nu_s(\text{CH}_2)$ and eq 6. ^b Calculated from the first moment of ²H NMR spectra using relation $M_1 = 3.047 \times 10^5 S_{\text{CD}}^{102}$ and the transformation given by eq 7. ^c Calculated from the average chain tilt angle. ^d Calculated from the angle between transition dipole and bilayer normal using eqs 6, 7, and 8.

where C is the capacity and d is the thickness of the bilayer. This pressure causes a change in the thickness Δd (thinning of the bilayer) which leads to an increase of $\langle\theta_{\text{chain}}\rangle$, as described by the equation⁹⁹

$$\Delta \cos \langle\theta_{\text{chain}}\rangle = - \frac{C(E - E_{\text{pzc}} - \phi_2)^2}{2lK} \quad (10)$$

where l is the chain length and K is the Young's modulus of elasticity of the membrane. Zawisza et al.⁵⁷ have estimated that, for a pure DMPC bilayer, the electrocompression may cause an increase in the tilt angle of $\sim 5^\circ$ for $(E - E_{\text{pzc}} - \phi_2) = -0.5$ V. In the presence of GD, the detachment of the bilayer begins when $(E - E_{\text{pzc}} - \phi_2) \approx -0.4$ V. Using the values of $l \approx 5$ nm and $K \approx 2 \times 10^7$ Pa reported in ref 57, we obtain an estimate of the change of the tilt angle caused by electrocompression of $\sim 3^\circ$ at $(E - E_{\text{pzc}} - \phi_2) = -0.4$ V, in good agreement with the data in Figure 7.

The values of S_{chain} and $\langle\theta_{\text{chain}}\rangle$ determined in this study for the bilayer supported on the gold electrode can be compared to the order parameter values reported for mixed DMPC/GD bilayers in ATR measurements for a stack of multiple bilayers,^{39,100} a film of dried liposomes,³⁷ and a monolayer supported at a germanium crystal.⁴⁴ In addition, the chain order parameter can also be determined from deuterium quadrupolar splitting (DQS) measured by NMR for deuterated phospholipids.⁹⁶ The deuterium quadrupolar splitting is proportional to the order parameter of the C-D bond from which the segmental order parameter can be calculated with the help of eq 7. However, the time associated with the measurement of the quadrupolar splitting is $\sim 10^{-5}$ s, while the time of the *trans/gauche* isomerization is approximately 10^{-10} s.^{100,101} Consequently, the order parameter measured by NMR is time and space averaged. In contrast, the molecular vibrations corresponding to IR bands have characteristic times of 10^{-13} – 10^{-14} s,

that are much shorter than the isomerization time, and the order parameter determined from IR spectra is only spatially averaged.¹⁰¹

Table 1 lists the values of the chain order parameter obtained from DQS and ATR spectroscopy for lipids in samples that contain GD, in addition to the values determined in the present work. The results show that the acyl chains in the bilayer supported at the gold electrode surface are less ordered or more tilted in the adsorbed state than in the multiple bilayers investigated by ATR or NMR. In contrast, the acyl chains are more ordered or less tilted in the desorbed state of the bilayer than in the samples investigated previously in the literature.

A larger tilt angle in the adsorbed state of the bilayer supported at gold is a result of the interaction between the polar heads and the metal surface, as explained by the cartoon in Figure 7. In the desorbed state, the bilayer is separated from the metal by a ~ 1 -nm-thick layer of electrolyte and these conditions are similar to those of a stack of hydrated bilayers. However, in this study the bilayer was formed by the transfer of monolayers compressed in a Langmuir trough at a high film pressure. Therefore, molecules are more compressed in our sample than in multiple bilayers that were cast by evaporation of organic solvent in which the lipid and the peptide were dissolved.

DMPC Carbonyl Group. The stretching vibration of the glycerol ester group provides useful information regarding the hydration of the lipid interfacial region as well as lipid–peptide interactions that involve the formation of hydrogen bonding. This band is quite broad and complex.¹⁰³ The overall shape and position of the C=O stretch depend on the hydration of the ester group. It may be seen as composed of two overlapping bands with maxima at approximately 1730 and 1740 cm^{-1} , which correspond to the presence of hydrogen-bonded and non-hydrogen-bonded ester groups, respectively.^{80,91,104,105}

Figure 8A plots the C=O stretch band in the supported bilayer formed by the LB-LS method at selected electrode potentials.

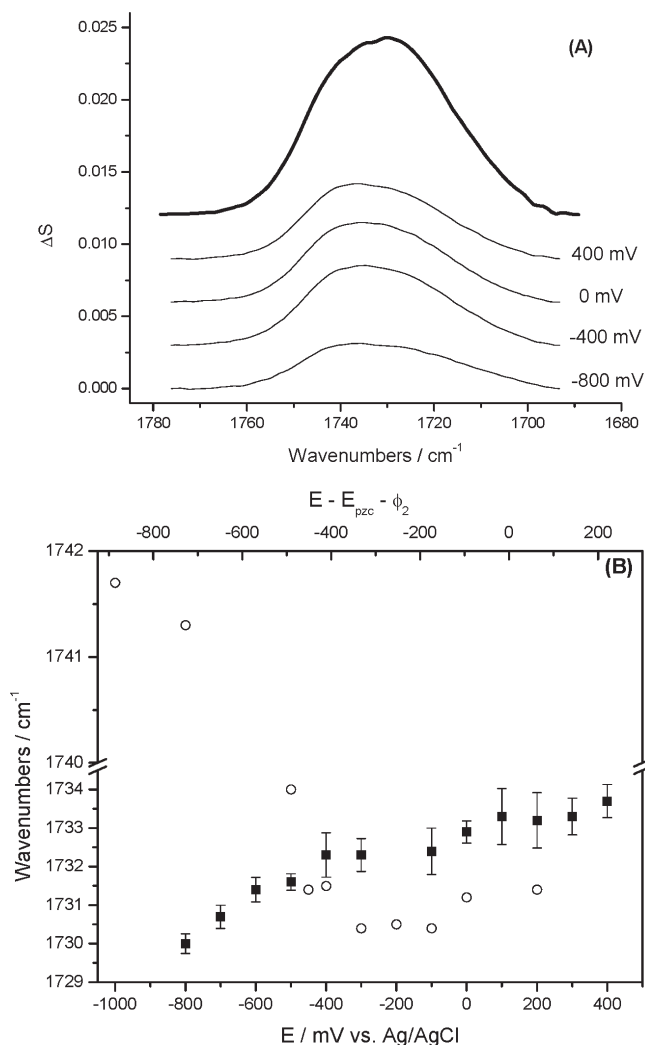


Figure 8. (A) Ester carbonyl stretching band ($\text{C}=\text{O}$)_s of the lipid in the DMPC/GD bilayer at selected electrode potentials. The thick line corresponds to the calculated spectrum of the DMPC molecules in a hypothetically randomly distributed DMPC/GD bilayer. (B) Frequency shift as a function of the electrode potential of the ($\text{C}=\text{O}$)_s band for the DMPC/GD bilayer (filled squares) and for a pure DMPC bilayer⁵⁷ (empty circles). The error bars correspond to the standard deviation calculated from 3 independent measurements.

The thick line corresponds to the calculated spectrum of the DMPC molecules in a randomly distributed DMPC/GD bilayer. In vesicle dispersions, the band has a maximum at approximately 1729 cm^{-1} . When the bilayer is supported, the peak maximum shifts to higher frequencies, indicating that the presence of the gold substrate dehydrates the membrane. The position of the band center is plotted as a function of the electrode potential in Figure 8B. At positive potentials (in the adsorbed state), the peak maximum lies at $\sim 1733\text{ cm}^{-1}$. At negative potentials, the band is red-shifted by $\sim 3\text{ cm}^{-1}$ upon desorption. This shift indicates that in the adsorbed state the $\text{C}=\text{O}$ groups of the lipid molecules are less involved in H-bond formation than in the desorbed (detached) state. In Figure SI 5A of the Supporting Information, the $\text{C}=\text{O}$ stretching band has been deconvoluted into high and low frequency components. Figure SI 5B shows that the positions of the deconvoluted bands are, within the experimental error, independent of the electrode potential. Therefore, the change

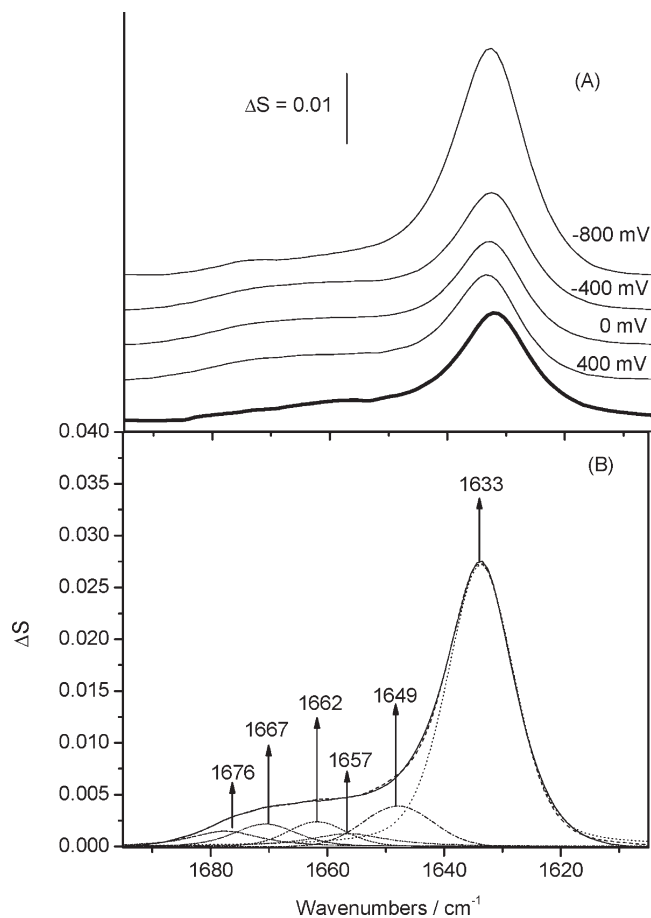


Figure 9. (A) PMIRRA spectra of the Amide I' of GD in a DMPC bilayer at $19\text{ }^{\circ}\text{C}$ transferred at 40 mN m^{-1} at selected potentials. The thick line corresponds to the spectrum calculated for hypothetically randomly oriented GD molecules in a 10% molar ratio in an 5.4-nm -thick DMPC/GD bilayer. (B) Deconvoluted spectrum of the Amide I' band of GD for a DMPC/GD bilayer at $E = -0.1\text{ V}$. The deconvolution is described in Figures SI 5 and 6 of the Supporting Information.

in the band position seen in Figure 8B results from the changing contribution of the non-hydrogen bonding and hydrogen bonding bands to the overall band shape, as illustrated by the data in Figure SI 5C. Open points in Figure 8B plot the $\text{C}=\text{O}$ stretch band position for the peptide free DMPC bilayer taken from ref 57. These data show that, in the absence of GD, the band center experiences a blue shift upon desorption, indicating that the $\text{C}=\text{O}$ groups become less hydrated. In a DMPC/GD membrane, hydrogen bonding of the DMPC carbonyl may involve water molecules or the amino acid side chains of the gramicidin.⁹ In the pure DMPC membrane, the carbonyl groups can only form hydrogen bonds with water. Solid-state NMR, Raman, and fluorescence spectroscopy have shown that the NH groups of the tryptophan indole rings point toward the carbonyl groups.^{106,107} According to molecular dynamic simulations of the gramicidin channel in a DMPC bilayer performed by Woolf and Roux,⁹ the indole rings of the tryptophans are involved in hydrogen bonds with the carbonyl groups of the DMPC molecule. It is therefore likely that the red shift seen in Figure 8B is due to increased hydrogen bonding between the lipid and the peptide's tryptophans upon desorption of the bilayer at negative potentials when the

system is less rigid due to the presence of a cushion of electrolyte between the film and the electrode.⁸¹

Amide I Band. The vibrational motions of peptide backbones give rise to the so-called amide bands. Of them, the Amide I (AmI) band is primarily a stretching of the C=O bond, together with a minor contribution from the out-of-phase CN stretching, CCN deformation, and the NH in-plane bend.¹⁰⁸ Figure 9 shows the PMIRRAS spectra of the amide I of GD in the mixed DMPC/GD bilayer at 19 °C transferred at 40 mN m⁻¹ at selected potentials indicated in the figure. The spectra were recorded in D₂O to avoid interference from water bands.

The thick line corresponds to the hypothetical spectrum of randomly oriented GD molecules in a 5.4-nm-thick bilayer with a 10% molar ratio of the peptide. The amide I band shows a main peak located at ~1634 cm⁻¹ and a higher frequency shoulder that extends for approximately 40 cm⁻¹. The force field normal mode calculations by Naik and Krimm¹⁰⁹ show that different conformations of GD appear under the amide I band. Since the spectra were recorded in D₂O, the frequencies here reported for the AmI' (note the apostrophe in the notation) band are red-shifted by about 6 cm⁻¹ with respect to those calculated by Naik and Krimm due to hydrogen/deuterium exchange of the labile amine hydrogens.¹¹⁰

The single-stranded conformation of GD $\beta^{6.3}$ occurs at lower frequencies and appears as a narrow peak whereas the double-stranded $\beta^{5.6}$ double helix is responsible for the higher frequency shoulder. Knowing how many peaks exist under the envelope of a spectral region of interest is not trivial. This is especially true for the Amide I band of GD, which is conformation sensitive. Fourier self-deconvolution (FSD) in conjunction with generalized two-dimensional correlation spectroscopy (2D-COS)^{88,111} was used to determine the number of peaks and their corresponding frequencies. This procedure is described in Figures SI 6 and 7 of the Supporting Information. Figure 9B shows that six sub-bands were identified under the envelope of the amide I' band. The low-frequency peak that is the main component of the Amide band at about 1633 cm⁻¹ corresponds to the helical dimer (HD) $\beta^{6.3}$. The smaller bands under the higher-frequency shoulder at about 1649, 1656, 1662, 1668, and 1675 cm⁻¹ correspond to hydrogen bonding patterns similar to those in $\beta^{5.6}$ double helices.^{42,109} However, this assignment is based on the normal mode calculations by Naik and Krimm that were performed for an infinite β -helix. Alternative interpretation of the origin of the high-frequency shoulder in the Amide I band of GD was given by Axelsen et al.,⁴⁴ Ulrich and Vogel,³⁵ and Owicki et al.¹¹² They assigned the shoulder to amide groups with weaker H-bonds at the head-to-head junction and possibly at the entrance of the channel. However, the data in Figure 9B demonstrate that the $\beta^{6.3}$ predominantly contributes to the intensity of the AmI' band. This is consistent with the circular dichroism studies of a stack of 10 DMPC-GD bilayers described in our earlier publication⁵³ which demonstrated that the HD conformation is prevalent in the DMPC membrane deposited at a gold electrode surface. We will analyze further the behavior of this band whose assignment is unambiguous.

Figure 10 plots the frequency of the deconvoluted main peak under the amide I band as a function of electrode potential. At positive potentials in the adsorbed state of the film, the peak is centered at ~1634 cm⁻¹. At negative potentials, where the bilayer is desorbed, the maximum of adsorption of the amide I band is located at ~1632 cm⁻¹. The amide I band frequency depends strongly on the intramolecular hydrogen bonding pattern and on the transition dipole coupling mechanism (TDC).¹⁰⁸

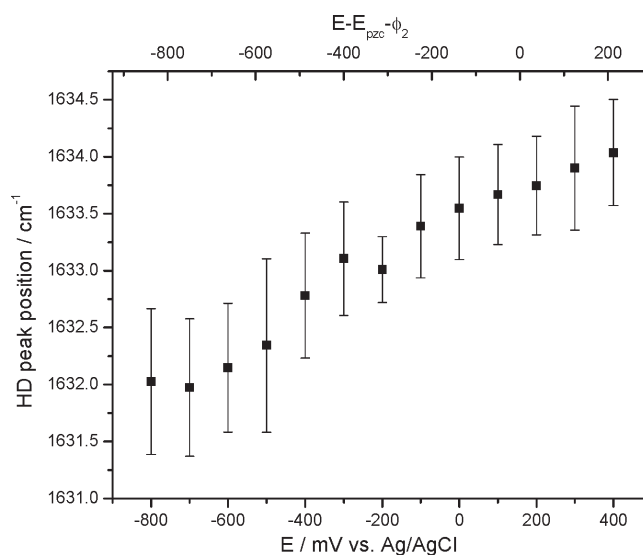


Figure 10. Frequency shift of the deconvoluted main peak under the Amide I' band as a function of electrode potential. The error bars correspond to the standard deviation calculated from 3 independent measurements.

The latter is the main mechanism that causes the amide I band to be sensitive to the secondary structure of the protein. The TDC involves interactions between the oscillating dipoles of neighboring amide groups that depend upon the relative orientation of and the distance between the dipoles. The blue shift of the amide I band indicates that the TDC and/or intramolecular hydrogen bonding are weakened in the adsorbed state. This suggests a change in the angle and/or in the distance between the oscillating dipoles of the amide groups when the bilayer is deposited at and in direct contact with the metal surface. The data in Figure 10 show that the GD molecule is stressed in the adsorbed state of the bilayer. The stress is relaxed when the bilayer is lifted and separated from the metal by a thin layer of electrolyte at negative potentials.

Orientation of the $\beta^{6.3}$ Helix. The integrated intensities of the amide I band and eq 4 allows one to determine the angle α between the direction of the transition dipole moment vector (μ) of the AmI' band and the surface normal. Knowing the angle α between the direction of the transition dipole moment of the amide I band and the helix axis, one can determine the orientation of GD molecules in the supported bilayer and investigate its change as a function of potential applied to the electrode. However, there is considerable uncertainty in the literature regarding the orientation of the transition dipole of the AmI vibration in the gramicidin molecule because the direction of the transition dipole depends on the helix structure.

Nabedryk et al.,³⁷ Okamura et al.,¹⁰⁰ and Bouchard and Auger⁴⁶ used a value of $\alpha = 22.6^\circ$ assuming the $\beta^{4.4}$ helix geometry. In contrast, Ulrich and Vogel³⁵ used a value of $\alpha = 10.8^\circ$ determined by Naik and Krimm¹⁰⁹ for the $\beta^{6.3}$ helix conformation and assuming that the vibrations polarized along the helix axis contribute predominantly to the band intensity. Recently, Kota et al.³⁹ demonstrated that the Amide I band of $\beta^{6.3}$ helix has contributions from vibrations polarized parallel and perpendicular to the helix axis and estimated the effective angle $\alpha = 32^\circ$. Clearly, determining the direction of the transition dipole moment is not trivial and a systematic error is inevitably associated with the tilt angles of the GD helix reported below. To

obtain these values, we followed the arguments of Kota et al.³⁹ and assumed that the angle of the effective transition dipole of the Amide I band with respect to the helix axis is equal to 32° .

Figure 11 plots the average tilt angle of the GD channel with respect to the surface normal as a function of electrode potential. For comparison, the tilt angle values of the DMPC acyl chains that are shown in Figure 7 are also included in Figure 11. The orientation of the peptide changes by about 10° in the potential range studied. In the adsorbed state, the average tilt of the GD helix is $25 \pm 2^\circ$. As the bilayer detaches from the surface, the peptide becomes more upright and the angle decreases to $12 \pm 2^\circ$. The error bars shown represent the standard deviation of three independent sets of data. Figure 11 shows that the change of the tilt angle of the helix with potential parallels the change of

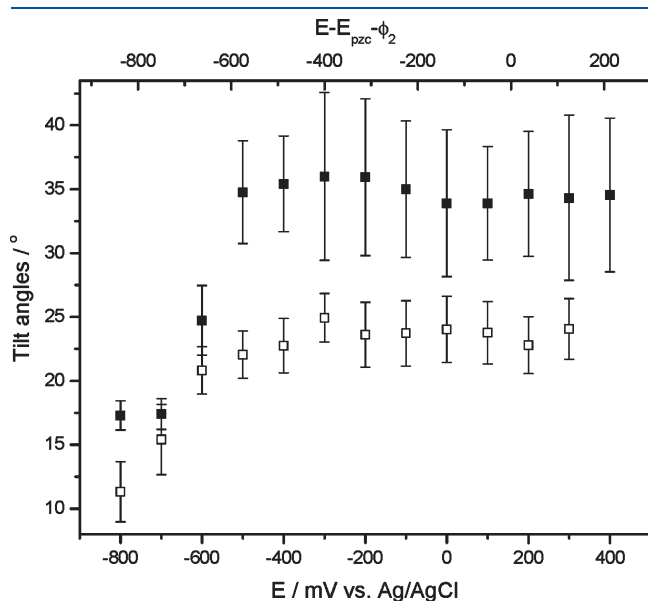


Figure 11. Average tilt angle of the GD channel (empty squares) with respect to the surface normal as a function of electrode potential calculated from the integrated band intensity and assuming an orientation of μ of 30° with respect to the helical axis. The orientation of the DMPC acyl chains (filled squares) is also plotted for comparison. The error bars correspond to the standard deviation of 3 independent sets of data.

the tilt of the acyl chains. In the case of the acyl chains, the change of the tilt angle between the adsorbed and desorbed states is driven by the difference in the packing of the polar heads of DMPC molecules in the two states. The corresponding change in the tilt of the helix can be explained in terms of the hydrophobic matching of the thickness of the hydrophobic portion of the bilayer to the length of the peptide.^{7,49,98} The energetic cost of hydrophobic mismatch is proportional to the square of the difference between the thickness of the bilayer and the projected length of the peptide in the direction normal to the bilayer.^{49,98} The bilayer responds to the hydrophobic stress by changing the tilt of the peptide to better accommodate it within the bilayer core. The length of two all-*trans* stretched acyl chains of DMPC molecules is 34 \AA . In the gel state, the maximum hydrophobic thickness of the bilayer is then given by the product of 34 \AA and $\cos \langle \theta_{\text{chain}} \rangle$, where θ_{chain} is the angle between the axis of the peptide and the bilayer normal. Hence, the bilayer hydrophobic thickness changes from $27 \pm 1 \text{ \AA}$ in the adsorbed state (corresponding to a tilt of $35^\circ \pm 2^\circ$) to $32 \pm 1 \text{ \AA}$ in the desorbed state (for an angle of $20^\circ \pm 3^\circ$). X-ray crystallographic data for the GD channel has shown that the gramicidin dimer length is 26 \AA (13 \AA per monomer).¹¹³ Taking into account the angles determined in this work, the GD channel spans a distance of $23.5 \pm 1 \text{ \AA}$ to $25.6 \pm 1 \text{ \AA}$ in the adsorbed and desorbed states, respectively. These values give the hydrophobic mismatch in these two states corresponding to $3.5 \pm 1 \text{ \AA}$ and $6 \pm 1 \text{ \AA}$, respectively. The hydrophobic matching appears to be better in the adsorbed state. However, the hydrophobic core thickness of the DMPC/GD bilayer is less than the above estimate, since the acyl chains are not in the all-*trans* conformation but are partially melted. Indeed, the thickness of a DMPC bilayer decreases by $\sim 5 \text{ \AA}$ by moving across the phase transition from the gel to the liquid crystalline state.^{114–117} This change is sufficient to match the hydrophobic thickness of the bilayer and the projected length of the peptide and to eliminate the hydrophobic stress.

Table 2 lists the tilt angle values obtained in the present study together with those reported previously for various DMPC/GD samples. There is a huge spread of the reported tilt angles of the helix. This spread may be explained by differences among (i) the direction of the transition dipole with respect to the helix axis, (ii) the nature of the sample (stack of multiple bilayers versus single bilayer versus a monolayer), and (iii) the temperature, and hence the acyl chain order of the phospholipid. Nonetheless, Table 2

Table 2. GD Orientation in DMPC/GD Samples Determined by Several Authors along with the Value of the Transition Dipole Moment Used in Their Calculation

DMPC/GD sample (temperature)	angle of the helix	Amide I transition dipole	angle of the lipid in DMPC/GD	IR method	ref
dry vesicles (room temperature)	$<15^\circ$	22.6°	11.5°	polarized transmission	37
monolayer at air/water interface (20°C)	31°	10.8°	N/A	PMIRRAS	35
hydrated multibilayers (30°C)	$32^\circ \pm 2^\circ$	22.6°	$\theta_{\text{chains}} = 25^\circ \pm 7^\circ$	polarized ATR	100
hydrated multibilayers (40°C)	$42^\circ \pm 2^\circ$	22.6°	$\theta_{\text{chains}} = 31^\circ \pm 1^\circ$	polarized ATR	46
hydrated multibilayers		32°	$\theta_{\text{chains}} = 33^\circ$	polarized ATR	39
10°C	$42^\circ \pm 2^\circ$				
40°C	$40^\circ \pm 2^\circ$				
hydrated multibilayers (34°C)	$16^\circ \pm 2^\circ$	N/A	N/A	NMR	30
phospholipid/GD (liquid crystalline state)	$12 \pm 6^\circ$	N/A	N/A	NMR	118
this work		30°		PMIRRAS	single bilayer at Au(111)
adsorbed state	$23^\circ \pm 2^\circ$		$\theta_{\text{chains}} = 35^\circ \pm 2^\circ$		
desorbed state	$12^\circ \pm 2^\circ$		$\theta_{\text{chains}} = 18^\circ \pm 3^\circ$		

shows that, for all of the stacks of hydrated multibilayers, the θ_{chain} values of DMPC molecules is smaller by $\sim 10^\circ$ than the θ_{helix} values of the peptide. Specifically, Kota et al.³⁹ used the same orientation of the transition dipole ($\alpha = 32^\circ$) as in our study. However, for the gel state of the bilayer (at 10°C) they reported values of $\theta_{\text{helix}} = 42^\circ$ and $\theta_{\text{chain}} = 33^\circ$. These values correspond to a hydrophobic mismatch of the order of 10 \AA and hence are not realistic. Our data are not in agreement with all the ATR studies of stacks of multiple bilayers reported in the literature. However, the value of θ_{helix} determined by us for the desorbed state, where the bilayer is separated from the metal by a $\sim 1\text{ nm}$ cushion of the electrolyte, is in excellent agreement with the NMR data.^{30,118}

SUMMARY AND CONCLUSIONS

We have provided rich new information on how the stability of the DMPC/GD bilayer supported at a gold electrode and the orientation and conformation of the phospholipid and peptide molecules depend on the potential drop across the membrane (transmembrane potential). We have compared the properties of the membrane containing peptide to the properties of the pure DMPC bilayer. The bilayer is adsorbed and in direct contact with the metal when the transmembrane potential is small. When a negative potential is applied across the membrane, it detaches the membrane from the metal and, at sufficiently negative potentials, it becomes separated from the metal by a thin, $\sim 1\text{-nm}$ -thick cushion of electrolyte. Therefore, the potential can be used to switch between the adsorbed and desorbed states of the bilayer. There are significant differences between the tilt of the acyl chains in the adsorbed (more tilted) and the desorbed (less tilted by about 17°) states of the bilayer caused by different packing of the polar head groups. In the detached state, the polar heads are packed in a zigzag fashion. In the adsorbed state, all polar heads are located in one plane in contact with the metal and hence occupy a larger surface area. The presence of 10% GD has a measurable impact on the bilayer behavior. The bilayer detaches at potentials about 100 mV less negative in the presence of GD, and the acyl chains of DMPC molecules are more tilted in the presence of GD. In addition, carbonyl groups of the glycerol moiety form more hydrogen bonds that most likely involve indol groups of the tryptophan side chains of GD.

The IR data indicated that the helical dimer ($\beta^{6.3}$) is the prevalent conformation of GD in the supported bilayer. The orientation of the helix axis changes with the potential in parallel with the change in the tilt of the acyl chains of the DMPC molecules. However, the average tilt of the helix is smaller than that of the DMPC chains by approximately 10° . The potential controlled change in the helix orientation can be explained by hydrophobic matching. The orientation of the chains and the peptide are optimized to ensure that the thickness of the hydrophobic portion of the bilayer and the projected length of the peptide on the bilayer normal are matched. Consequently, the tilt angle of the helix is about 23° in the adsorbed state, which is about 10° more than in the desorbed state. At such a large tilt angle, the helix is stressed and small changes in the strength of its bonds and bond angles occur which cause a blue shift of the amide I band of the helix. The stress is relaxed in the desorbed state.

In conclusion, we have demonstrated that gold-supported model membranes offer a unique opportunity to perform combined electrochemical and spectroscopic studies. This approach provides new molecular level information about the

properties of the peptide containing membranes exposed to static electric fields that are comparable to the fields acting on a natural biological membrane.

ASSOCIATED CONTENT

S Supporting Information. AFM images of the DMPC/GD bilayer before and after annealing, Figure SI 1; Isotropic optical constants for DMPC/GD (10:1) system, Figure SI 2; Fourier self-deconvolution of the CH stretch region of the IR spectra, Figure SI 3; Angle between the transition dipole of the CH_2 bending mode and surface normal, Figure SI 4; Deconvolution of the C=O band into the non hydrogen bonding (high frequency) and hydrogen bonding (low frequency) bands, dependence on potential of the deconvoluted band positions and the ratio of the high frequency band area to the overall area of the C=O band, Figure SI 5; Fourier self-deconvolution of the Amide I' band, Figure SI 6; 2D-COS analysis of the Amide I' band, Figure SI 7; Figure SI 8 description of the error propagation analysis for the tilt angles. This material is available free of charge via the Internet at <http://pubs.acs.org>.

AUTHOR INFORMATION

Present Addresses

⁵Departments of Interdisciplinary Studies and Chemistry, Lakehead University, Orillia, Ontario, L3V 0B9, Canada.

ACKNOWLEDGMENT

This work was supported by grants from the Natural Sciences and Engineering Research Council of Canada and the Advanced Foods and Materials Network. J.R.D. and J.L. acknowledge support from the Canada Research Chairs (CRC) program.

REFERENCES

- (1) Moran, M. M.; Xu, H.; Clapham, D. E. TRP ion channels in the nervous system. *Curr. Opin. Neurobiol.* **2004**, *14*, 362–369.
- (2) Hille, B. In *Ion channels of excitable membranes*; Sinauer Publishers: MA, 2001; p 814.
- (3) Hancock, R. E. W.; Chapple, D. S. Peptide antibiotics. *Antimicrob. Agents Chemother.* **1999**, *43*, 1317.
- (4) Finlay, B. B.; Hancock, R. E. W. Can innate immunity be enhanced to treat microbial infections? *Nat. Rev. Microbio.* **2004**, *2*, 497–504.
- (5) Hancock, R. E. W.; Patrzykat, A. Clinical development of cationic antimicrobial peptides: from natural to novel antibiotics. *Curr. Drug Targets Infect. Disorders* **2002**, *2*, 79–83.
- (6) Cornell, B. A.; Braach-Maksvytis, V. L. B.; King, L. G.; Osman, P. D. J.; Raguse, B.; Wiczorek, L.; Pace, R. J. A biosensor that uses ion-channel switches. *Nature* **1997**, 580–582.
- (7) Kelkar, D. A.; Chattopadhyay, A. The gramicidin ion channel: A model membrane protein. *Biochim. Biophys. Acta* **2007**, *1768*, 2011–2025.
- (8) Andersen, O. S.; Koeppe, R. E.; Roux, B. Gramicidin channels. *IEEE Trans. NanoBiosci.* **2005**, *4*, 10–20.
- (9) Woolf, T. B.; Roux, B. Structure, energetics, and dynamics of lipid-protein interactions: A molecular dynamics study of the gramicidin A channel in a DMPC bilayer. *Prot. Struct. Funct. Gen.* **1996**, *24*, 92–114.
- (10) Wallace, B. A. Gramicidin Channels and Pores. *Annu. Rev. Biophys. Chem.* **1990**, *19*, 127–157.
- (11) Urry, D. W. A molecular theory of ion-conducting channels: a field-dependent transition between conducting and nonconducting conformations. *Proc. Natl. Acad. Sci. U. S. A.* **1972**, *69*, 1610–1614.

- (12) Sandblom, J.; Galvanovskis, J.; Jilderos, B. Voltage-dependent formation of gramicidin channels in lipid bilayers. *Biophys. J.* **2001**, *81*, 827–837.
- (13) Wallace, B. A. Recent advances in the high resolution structures of bacterial channels: Gramicidin A. *J. Struct. Biol.* **1998**, *121*, 123–141.
- (14) Hladky, S. B.; Haydon, D. A. Ion transfer across lipid membranes in the presence of gramicidin A. I. Studies of the unit conductance channel. *Biochim. Biophys. Acta* **1972**, *274*, 294–312.
- (15) Busath, D. D.; Thulin, C. D.; Hendershot, R. W.; Phillips, L. R.; Maughan, P.; Cole, C. D.; Bingham, N. C.; Morrison, S.; Baird, L. C.; Hendershot, R. J. Noncontact dipole effects on channel permeation. I. Experiments with (5F-indole) Trp13 gramicidin A channels. *Biophys. J.* **1998**, *75*, 2830–2844.
- (16) Woolley, G. A.; Zunic, V.; Karanicolas, J.; Jaikaran, A. S.; Starostin, A. V. Voltage-dependent behavior of a “ball-and-chain” gramicidin channel. *Biophys. J.* **1997**, *73*, 2465–2475.
- (17) Becucci, L.; Santucci, A.; Guidelli, R. Gramicidin conducting dimers in lipid bilayers are stabilized by single-file ionic flux along them. *J. Phys. Chem. B* **2007**, *111*, 9814–9820.
- (18) Becucci, L.; Innocenti, M.; Salvietti, E.; Rindi, A.; Pasquini, I.; Vassalli, M.; Foresti, M. L.; Guidelli, R. Potassium ion transport by gramicidin and valinomycin across a Ag (111)-supported tethered bilayer lipid membrane. *Electrochim. Acta* **2008**, *53*, 6372–6379.
- (19) He, L.; Robertson, J. W. F.; Li, J.; Kärcher, I.; Schiller, S. M.; Knoll, W.; Naumann, R. Tethered bilayer lipid membranes based on monolayers of thioliids mixed with a complementary dilution molecule. I. Incorporation of channel peptides. *Langmuir* **2005**, *21*, 11666–11672.
- (20) Vallejo, A. E.; Gervasi, C. A. Impedance analysis of ion transport through gramicidin channels in supported lipid bilayers. *Bioelectrochemistry* **2002**, *57*, 1–7.
- (21) Steinem, C.; Janshoff, A.; Galla, H. J.; Sieber, M. Impedance analysis of ion transport through gramicidin channels incorporated in solid supported lipid bilayers. *Bioelectrochem. Bioenerget.* **1997**, *42*, 213–220.
- (22) Nelson, A.; Benton, A. Phospholipid monolayers at the mercury/water interface. *J. Electroanal. Chem.* **1986**, *202*, 253–270.
- (23) Nelson, A. Conducting gramicidin channel activity in phospholipid monolayers. *Biophys. J.* **2001**, *80*, 2694–2703.
- (24) Nelson, A.; Bizzotto, D. Chronoamperometric study of TI (I) reduction at gramicidin-modified phospholipid-coated mercury electrodes. *Langmuir* **1999**, *15*, 7031–7039.
- (25) Rueda, M.; Prieto, F.; Navarro, I.; Romero, R. Phospholipid and gramicidin-phospholipid-coated mercury electrodes as model systems of partially blocked electrodes. *J. Electroanal. Chem.* **2010**.
- (26) Rueda, M.; Navarro, I.; Ramirez, G.; Prieto, F.; Prado, C.; Nelson, A. Electrochemical impedance study of TI reduction through gramicidin channels in self-assembled gramicidin-modified dioleoylphosphatidylcholine monolayers on mercury electrodes. *Langmuir* **1999**, *15*, 3672–3678.
- (27) Mauzeroll, J.; Buda, M.; Bard, A. J.; Prieto, F.; Rueda, M. Detection of TI (I) transport through a gramicidin-dioleoylphosphatidylcholine monolayer using the substrate generation-tip collection mode of scanning electrochemical microscopy. *Langmuir* **2002**, *18*, 9453–9461.
- (28) Morrow, M. R.; Davis, J. H. Differential scanning calorimetry and deuterium NMR studies of the phase behavior of gramicidin-phosphatidylcholine mixtures. *Biochemistry* **1988**, *27*, 2024–2032.
- (29) Prosser, R. S.; Daleman, S. I.; Davis, J. H. The structure of an integral membrane peptide: a deuterium NMR study of gramicidin. *Biophys. J.* **1994**, *66*, 1415–1428.
- (30) Prosser, R. S.; Davis, J. H. Dynamics of an integral membrane peptide: a deuterium NMR relaxation study of gramicidin. *Biophys. J.* **1994**, *66*, 1429–1440.
- (31) Kobayashi, Y.; Fukada, K. Characterization of swollen lamellar phase of dimyristoylphosphatidylcholine—gramicidin A mixed membranes by DSC, SAXS, and densimetry. *Biochim. Biophys. Acta* **1998**, *1371*, 363–370.
- (32) Killian, J. A.; Prasad, K. U.; Hains, D.; Urry, D. W. The membrane as an environment of minimal interconversion. A circular dichroism study on the solvent dependence of the conformational behavior of gramicidin in diacylphosphatidylcholine model membranes. *Biochemistry* **1988**, *27*, 4848–4855.
- (33) Wallace, B. A.; Veatch, W. R.; Blout, E. R. Conformation of gramicidin A in phospholipid vesicles: circular dichroism studies of effects of ion binding, chemical modification, and lipid structure. *Biochem.* **1981**, *20*, 5754–5760.
- (34) Weis, M.; Vanco, M.; Vitovic, P.; Hianik, T.; Cirak, J. Study of Gramicidin A-phospholipid interactions in langmuir monolayers: analysis of their mechanical, thermodynamical, and electrical properties. *J. Phys. Chem. B* **2006**, *110*, 26272–26278.
- (35) Ulrich, W. P.; Vogel, H. Polarization-modulated FTIR spectroscopy of lipid/gramicidin monolayers at the air/water interface. *Biophys. J.* **1999**, *76*, 1639–1647.
- (36) Leonenko, Z. V.; Carnini, A.; Cramb, D. T. Supported planar bilayer formation by vesicle fusion: the interaction of phospholipid vesicles with surfaces and the effect of gramicidin on bilayer properties using atomic force microscopy. *Biochim. Biophys. Acta* **2000**, *1509*, 131–147.
- (37) Nabedryk, E.; Gingold, M. P.; Breton, J. Orientation of gramicidin A transmembrane channel. Infrared dichroism study of gramicidin in vesicles. *Biophys. J.* **1982**, *38*, 243–249.
- (38) Lukes, P. J.; Petty, M. C.; Yarwood, J. An infrared study of the incorporation of ion channel forming peptides into Langmuir-Blodgett films of phosphatidic acid. *Langmuir* **1992**, *8*, 3043–3050.
- (39) Kota, Z.; Pali, T.; Marsh, D. Orientation and lipid-peptide interactions of Gramicidin A in lipid membranes: polarized attenuated total reflection infrared spectroscopy and spin-label electron spin resonance. *Biophys. J.* **2004**, *86*, 1521–1531.
- (40) Lee, D. C.; Durrani, A. A.; Chapman, D. A difference infrared spectroscopic study of gramicidin A, alamethicin and bacteriorhodopsin in perdeuterated dimyristoylphosphatidylcholine. *Biochim. Biophys. Acta* **1984**, *769*, 49–56.
- (41) Davies, M. A.; Brauner, J. W.; Schuster, H. F.; Mendelsohn, R. A quantitative infrared determination of acyl chain conformation in gramicidin/dipalmitoylphosphatidylcholine mixtures. *Biochem. Biophys. Res. Commun.* **1990**, *168*, 85–90.
- (42) Zein, M.; Winter, R. Effect of temperature, pressure and lipid acyl chain length on the structure and phase behaviour of phospholipid—gramicidin bilayers. *Phys. Chem. Chem. Phys.* **2000**, *2*, 4545–4551.
- (43) Ha, J.; Henry, C. S.; Fritsch, I. Formation and characterization of supported hexadecanethiol/dimyristoyl phosphatidylcholine hybrid bilayers containing Gramicidin D. *Langmuir* **1998**, *14*, 5850–5857.
- (44) Axelsen, P. H.; Kaufman, B. K.; McElhaney, R. N.; Lewis, R. N. The infrared dichroism of transmembrane helical polypeptides. *Biophys. J.* **1995**, *69*, 2770–2781.
- (45) Bouchard, M.; Benjamin, D. R.; Tito, P.; Robinson, C. V.; Dobson, C. M. Solvent effects on the conformation of the transmembrane peptide Gramicidin A: insights from electrospray ionization mass spectrometry. *Biophys. J.* **2000**, *78*, 1010–1017.
- (46) Bouchard, M.; Auger, M. Solvent history dependence of gramicidin-lipid interactions: a Raman and infrared spectroscopic study. *Biophys. J.* **1993**, *65*, 2484–2492.
- (47) Killian, J. A. Gramicidin and gramicidin-lipid interactions. *Biochim. Biophys. Acta* **1992**, *1113*, 391–425.
- (48) Ohvo-Rekilä, H.; Ramstedt, B.; Leppimäki, P.; Peter Slotte, J. Cholesterol interactions with phospholipids in membranes. *Prog. Lipid Res.* **2002**, *41*, 66–97.
- (49) Harroun, T. A.; Heller, W. T.; Weiss, T. M.; Yang, L.; Huang, H. W. Experimental evidence for hydrophobic matching and membrane-mediated interactions in lipid bilayers containing Gramicidin. *Biophys. J.* **1999**, *76*, 937–945.
- (50) de Planque, M. R. R.; Killian, J. A. Protein-lipid interactions studied with designed transmembrane peptides: role of hydrophobic matching and interfacial anchoring (Review). *Mol. Membr. Biol.* **2003**, *20*, 271–284.
- (51) Killian, J. A.; Borle, F.; de Kruijff, B.; Seelig, J. Comparative 2H- and 31P-NMR study on the properties of palmitoyllysophosphatidylcholine in bilayers with gramicidin, cholesterol and dipalmitoylphosphatidylcholine. *Biochim. Biophys. Acta* **1986**, *854*, 133–142.

- (52) Sek, S.; Laredo, T.; Dutcher, J. R.; Lipkowski, J. Molecular resolution imaging of an antibiotic peptide in a lipid matrix. *J. Am. Chem. Soc.* **2009**, *131*, 6439–6444.
- (53) Fiche, J. B.; Laredo, T.; Tanchak, O.; Lipkowski, J.; Dutcher, J. R.; Yada, R. Y. Influence of an electric field on oriented films of DMPC/Gramicidin bilayers: a circular dichroism study. *Langmuir* **2009**, *26*, 1057–1066.
- (54) Brosseau, C. L.; Bin, X.; Roscoe, S. G.; Lipkowski, J. Electrochemical and PM-IRRAS characterization of DMPC+cholesterol bilayers prepared using Langmuir-Blodgett/Langmuir-Schaefer deposition. *J. Electroanal. Chem.* **2008**, *621*, 222–228.
- (55) Brosseau, C. L.; Leitch, J.; Bin, X.; Chen, M.; Roscoe, S. G.; Lipkowski, J. Electrochemical and PM-IRRAS a glycolipid-containing biomimetic membrane prepared using Langmuir-Blodgett/Langmuir-Schaefer deposition. *Langmuir* **2008**, *24*, 13058–13067.
- (56) Matyszewska, D.; Leitch, J.; Bilewicz, R.; Lipkowski, J. Polarization modulation infrared reflection—absorption spectroscopy studies of the influence of perfluorinated compounds on the properties of a model biological membrane. *Langmuir* **2008**, *24*, 7408–7412.
- (57) Zawisza, I.; Bin, X.; Lipkowski, J. Potential-driven structural changes in Langmuir-Blodgett DMPC bilayers determined by in situ spectroelectrochemical PM IRRAS. *Langmuir* **2007**, *23*, 5180–5194.
- (58) Bin, X.; Lipkowski, J. Electrochemical and PM-IRRAS studies of the effect of cholesterol on the properties of the headgroup region of a DMPC bilayer supported at a Au (111) electrode. *J. Phys. Chem. B* **2006**, *110*, 26430.
- (59) Garcia-Araez, N.; Brosseau, C. L.; Rodriguez, P.; Lipkowski, J. Layer-by-Layer PMIRRAS characterization of DMPC bilayers deposited on a Au (111) electrode surface. *Langmuir* **2006**, *22*, 10365–10371.
- (60) Zawisza, I.; Wittstock, G.; Boukherroub, R.; Szunerits, S. Polarization modulation infrared reflection absorption spectroscopy investigations of thin silica films deposited on gold. 2. Structural analysis of a 1,2-dimyristoyl-sn-glycero-3-phosphocholine bilayer. *Langmuir* **2008**, *24*, 3922–3929.
- (61) Zawisza, I.; Nullmeier, M.; Pust, S. E.; Boukherroub, R.; Szunerits, S.; Wittstock, G. Application of thin titanium/titanium oxide layers deposited on gold for infrared reflection absorption spectroscopy: structural studies of lipid bilayers. *Langmuir* **2008**, *24*, 7378–7387.
- (62) Nullmeier, M.; Koliwer-Brandl, H.; Kelm, S.; Zägel, P.; Koch, K. W.; Brand, I. Impact of strong and weak lipid–protein interactions on the structure of a lipid bilayer on a gold electrode surface. *ChemPhysChem* **2011**, *12*, 1066–1079.
- (63) Röefzaad, M.; Klüner, T.; Brand, I. Orientation of the GM1 ganglioside in Langmuir–Blodgett monolayers: a PM IRRAS and computational study. *Phys. Chem. Chem. Phys.* **2009**, *11*, 10140–10151.
- (64) Hillman, A. R.; Ryder, K. S.; Madrid, E.; Burley, A. W.; Wiltshire, R. J.; Merotra, J.; Grau, M.; Horswell, S. L.; Gidde, A.; Dalglish, R. M. Structure and dynamics of phospholipid bilayer films under electrochemical control. *Faraday Discuss.* **2009**, *145*, 357–379.
- (65) Zawisza, I.; Wittstock, G.; Boukherroub, R.; Szunerits, S. PM IRRAS investigation of thin silica films deposited on gold. Part I. Theory and proof of concept. *Langmuir* **2007**, *23*, 9303–9309.
- (66) Nullmeier, M.; Koliwer-Brandl, H.; Kelm, S.; Brand, I. Interaction of siglec protein with glycolipids in a lipid bilayer deposited on a gold electrode surface. *J. Electroanal. Chem.* **2010**, *649*, 177–188.
- (67) Brand, I.; Nullmeier, M.; Koliwer-Brandl, H.; Kelm, S. Abstracts on the 4th ISN Special Conference on “Membrane Domains in CNS Physiology and Pathology”, MAY 22–26, 2010 Erice, ITALY. *J. Neurochem.* **2010**, *113*, 1–32.
- (68) Barenholz, Y.; Gibbes, D.; Litman, B. J.; Goll, J.; Thompson, T. E.; Carlson, F. D. A simple method for the preparation of homogeneous phospholipid vesicles. *Biochem.* **1977**, *16*, 2806–2810.
- (69) Richer, J.; Lipkowski, J. Quantitative investigations of the adsorption of tert-amyl alcohol at the Au (100)/aqueous solution interface. *J. Electroanal. Chem. Interfacial Electrochem.* **1988**, *251*, 217–234.
- (70) Hamelin, A. In *Modern aspects of electrochemistry*, Conway, B., White, R. E., Bockris, J. O., Eds.; Plenum Press: New York, 1985; Vol 16.
- (71) Richer, J.; Lipkowski, J. Measurement of physical adsorption of neutral organic species at solid electrodes. *J. Electrochem. Soc.* **1986**, *133*, 121.
- (72) Li, N.; Zamlynyy, V.; Lipkowski, J.; Henglein, F.; Pettinger, B. In situ IR reflectance absorption spectroscopy studies of pyridine adsorption at the Au (110) electrode surface. *J. Electroanal. Chem.* **2002**, *524*, 43–53.
- (73) Buffeteau, T.; Desbat, B.; Blaudez, D.; Turlet, J. M. Calibration procedure to derive IRRAS spectra from PM-IRRAS spectra. *Appl. Spectrosc.* **2000**, *54*, 1646–1650.
- (74) Zamlynyy, V.; Zawisza, I.; Lipkowski, J. PM FTIRRAS studies of potential-controlled transformations of a monolayer and a bilayer of 4-pentadecylpyridine, a model surfactant, adsorbed on a Au (111) electrode surface. *Langmuir* **2003**, *19*, 132–145.
- (75) Barner, B. J.; Green, M. J.; Saez, E. I.; Corn, R. M. Polarization modulation Fourier transform infrared reflectance measurements of thin films and monolayers at metal surfaces utilizing real-time sampling electronics. *Anal. Chem.* **1991**, *63*, 55–60.
- (76) Green, M. J.; Barner, B. J.; Corn, R. M. Real-time sampling electronics for double modulation experiments with Fourier transform infrared spectrometers. *Rev. Sci. Instrum.* **1991**, *62*, 1426.
- (77) Czarniecki, M. A. Interpretation of two-dimensional correlation spectra: Science or art? *Appl. Spectrosc.* **1998**, *52*, 1583–1590.
- (78) Fringeli, U. P.; Gunthard, H. H. Infrared membrane spectroscopy. *Mol. Biol. Biochem. Biophys.* **1981**, *31*, 270–332.
- (79) Fringeli, P. U. The structure of lipids and proteins studied by attenuated total reflection (ATR) infrared spectroscopy. *Z. Naturforsch.* **1977**, *32*, 20–45.
- (80) Blume, A.; Hübner, W.; Messner, G. Fourier transform infrared spectroscopy of ¹³C: O labeled phospholipids hydrogen bonding to carbonyl groups. *Biochemistry* **1988**, *27*, 8239–8249.
- (81) Burgess, I.; Li, M.; Horswell, S. L.; Szymanski, G.; Lipkowski, J.; Majewski, J.; Satija, S. Electric field-driven transformations of a supported model biological membrane—an electrochemical and neutron reflectivity study. *Biophys. J.* **2004**, *86*, 1763–1776.
- (82) Bin, X.; Horswell, S. L.; Lipkowski, J. Electrochemical and PM-IRRAS studies of the effect of cholesterol on the structure of a DMPC bilayer supported at an Au (111) electrode surface, part I: Properties of the acyl chains. *Biophys. J.* **2005**, *89*, 592–604.
- (83) Jing, N.; Prasad, K. U.; Urry, D. W. The determination of binding constants of micellar-packaged gramicidin A by ¹³C- and ²³Na-NMR. *Biochim. Biophys. Acta* **1995**, *1238*, 1–11.
- (84) Woolf, T. B.; Roux, B. The binding site of sodium in the gramicidin A channel: comparison of molecular dynamics with solid-state NMR data. *Biophys. J.* **1997**, *72*, 1930–1945.
- (85) Mohilner, D. M. The electrical double layer; In Bard, A., Ed.; *Electroanalytical Chemistry*; Marcel Dekker: New York, 1966; Vol 11, pp 241–408.
- (86) Tsong, T.; Astumian, R. D. Electroconformational coupling: how membrane-bound ATPase transduces energy from dynamic electric fields. *Annu. Rev. Physiol.* **1988**, *50*, 273–290.
- (87) Zamlynyy, V. PhD Dissertation: Electrochemical and spectroscopic studies of pyridine surfactants at the gold-electrolyte interface; 2002.
- (88) Noda, I. Two-dimensional infrared (2D IR) spectroscopy: theory and applications. *Appl. Spectrosc.* **1990**, *44*, 550–561.
- (89) MacPhail, R. A.; Strauss, H. L.; Snyder, R. G.; Elliger, C. A. Carbon-hydrogen stretching modes and the structure of n-alkyl chains. 2. Long, all-trans chains. *J. Phys. Chem.* **1984**, *88*, 334–341.
- (90) Casal, H. L.; Mantsch, H. H. Polymorphic phase behaviour of phospholipid membranes studied by infrared spectroscopy. *Biochim. Biophys. Acta* **1984**, *779*, 381–401.
- (91) Mantsch, H. H.; McElhane, R. N. Phospholipid phase transitions in model and biological membranes as studied by infrared spectroscopy. *Chem. Phys. Lipids* **1991**, *57*, 213–226.
- (92) Mitchell, M. L.; Dluhy, R. A. In situ FT-IR investigation of phospholipid monolayer phase transitions at the air water interface. *J. Am. Chem. Soc.* **1988**, *110*, 712–718.
- (93) Allara, D. L.; Swalen, J. D. An infrared reflection spectroscopy study of oriented cadmium arachidate monolayer films on evaporated silver. *J. Phys. Chem.* **1982**, *86*, 2700–2704.
- (94) Allara, D. L.; Nuzzo, R. G. Spontaneously organized molecular assemblies. 2. Quantitative infrared spectroscopic determination of

equilibrium structures of solution-adsorbed n-alkanoic acids on an oxidized aluminum surface. *Langmuir* **1985**, *1*, 52–66.

(95) Binder, H.; Kohlstrunk, B. Infrared dichroism investigations on the acyl chain ordering in lamellar structures II. The effect of diene groups in membranes of dioctadecadienoylphosphatidylcholine. *Vibr. Spectrosc.* **1999**, *21*, 75–95.

(96) Seelig, J.; Niederberger, W. Deuterium-labeled lipids as structural probes in liquid crystalline bilayers. Deuterium magnetic resonance study. *J. Am. Chem. Soc.* **1974**, *96*, 2069–2072.

(97) Morrow, M. R.; Davis, J. H. Differential scanning calorimetry and deuterium NMR studies of the phase behavior of gramicidin-phosphatidylcholine mixtures. *Biochemistry* **1988**, *27*, 2024–2032.

(98) Harroun, T. A.; Heller, W. T.; Weiss, T. M.; Yang, L.; Huang, H. W. Theoretical analysis of hydrophobic matching and membrane-mediated interactions in lipid bilayers containing gramicidin. *Biophys. J.* **1999**, *76*, 3176–3185.

(99) Hianik, T. Electrostriction and dynamics of solid supported lipid films. *Rev. Mol. Biotechnol.* **2000**, *74*, 189–205.

(100) Okamura, E.; Umemura, J.; Takenaka, T. Orientation of gramicidin D incorporated into phospholipid multibilayers: a Fourier transform infrared-attenuated total reflection spectroscopic study. *Biochim. Biophys. Acta* **1986**, *856*, 68–75.

(101) Kodati, V. R.; Lafleur, M. Comparison between orientational and conformational orders in fluid lipid bilayers. *Biophys. J.* **1993**, *64*, 163–170.

(102) Davis, J. H. Deuterium magnetic resonance study of the gel and liquid crystalline phases of dipalmitoyl phosphatidylcholine. *Biophys. J.* **1979**, *27*, 339–358.

(103) Bin, X.; Zawisza, I.; Goddard, J. D.; Lipkowski, J. Electrochemical and PM-IRRAS studies of the effect of the static electric field on the structure of the DMPC bilayer supported at a Au (111) electrode surface. *Langmuir* **2005**, *21*, 330–347.

(104) Lewis, R.; McElhaney, R. N.; Pohle, W.; Mantsch, H. H. Components of the carbonyl stretching band in the infrared spectra of hydrated 1, 2-diacylglycerolipid bilayers: a reevaluation. *Biophys. J.* **1994**, *67*, 2367–2375.

(105) Hübner, W.; Blume, A. Interactions at the lipid-water interface. *Chem. Phys. Lipids* **1998**, *96*, 99–123.

(106) Hu, W.; Cross, T. A. Tryptophan hydrogen bonding and electric dipole moments: functional roles in the gramicidin channel and implications for membrane proteins. *Biochem.* **1995**, *34*, 14147–14155.

(107) Lin, T. H.; Huang, H. B.; Wei, H. A.; Shiao, S. H.; Chen, Y. C. The effect of temperature and lipid on the conformational transition of gramicidin A in lipid vesicles. *Biopolymers* **2005**, *78*, 179–186.

(108) Barth, A.; Zscherp, C. What vibrations tell about proteins. *Q. Rev. Biophys.* **2002**, *35*, 369–430.

(109) Naik, V. M.; Krimm, S. Vibrational analysis of the structure of gramicidin A. I. Normal mode analysis. *Biophys. J.* **1986**, *49*, 1131–1145.

(110) Tamm, L. K.; Tatulian, S. A. Infrared spectroscopy of proteins and peptides in lipid bilayers. *Q. Rev. Biophys.* **1997**, *30*, 365–429.

(111) Noda, I.; Ozaki, Y. In *Two-Dimensional Correlation Spectroscopy: Applications in Vibrational and Optical Spectroscopy*; John Wiley & Sons: Great Britain, 2004; p 295.

(112) Owicki, J. C.; Springgate, M. W.; McConnell, H. M. Theoretical study of protein-lipid interactions in bilayer membranes. *Proc. Natl. Acad. Sci. U. S. A.* **1978**, *75*, 1616–1619.

(113) Koeppe, R. E.; Berg, J. M.; Hodgson, K. O.; Stryer, L. Gramicidin A crystals contain two cation binding sites per channel. *Nature* **1979**, *279*, 723–725.

(114) Janiak, M. J.; Small, D. M.; Shipley, G. G. Nature of the thermal pretransition of synthetic phospholipids: dimyristoyl- and dipalmitoyllecithin. *Biochemistry* **1976**, *15*, 4575–4580.

(115) Tristram-Nagle, S.; Liu, Y.; Legleiter, J.; Nagle, J. F. Structure of gel phase DMPC determined by x-ray diffraction. *Biophys. J.* **2002**, *83*, 3324–3335.

(116) Pencer, J.; Nieh, M. -; Harroun, T. A.; Krueger, S.; Adams, C.; Katsaras, J. Bilayer thickness and thermal response of dimyristoylphosphatidylcholine unilamellar vesicles containing cholesterol, ergosterol

and lanosterol: A small-angle neutron scattering study. *Biochim. Biophys. Acta* **2005**, *1720*, 84–91.

(117) Chen, M.; Li, M.; Brosseau, C. L.; Lipkowski, J. AFM studies of the effect of temperature and electric field on the structure of a DMPC–cholesterol bilayer supported on a Au(111) electrode surface. *Langmuir* **2009**, *25*, 1028–1037.

(118) Separovic, F.; Pax, R.; Cornell, B. NMR order parameter analysis of a peptide plane aligned in a lyotropic liquid crystal. *Mol. Phys.* **1993**, *78*, 357–369.